The Geological Society of America
Special Paper 513
2015

Composite Sunrise Butte pluton: Insights into Jurassic–Cretaceous collisional tectonics and magmatism in the Blue Mountains Province, northeastern Oregon

Kenneth Johnson
Department of Natural Sciences, University of Houston–Downtown, 1 Main Street, Houston, Texas 77002, USA

Joshua J. Schwartz
Department of Geological Sciences, California State University–Northridge, 18111 Nordhoff Street, Northridge, California 91330, USA

Jiří Žák
Institute of Geology and Paleontology, Faculty of Science, Charles University, Albertov 6, Prague, 12843, Czech Republic

Kryštof Verner
Czech Geological Survey, Klárov 3, Prague, 11821, Czech Republic, and
Institute of Petrology and Structural Geology, Faculty of Science, Charles University, Albertov 6, Prague, 12843, Czech Republic

Calvin G. Barnes
Clay Walton
Department of Geosciences, Texas Tech University, MS 1053, Lubbock, Texas 79409-1053, USA

Joseph L. Wooden
U.S. Geological Survey–Stanford Ion Microprobe Laboratory, Stanford University, Stanford, California 94305-2220, USA

James E. Wright
Department of Geology, University of Georgia, 210 Field Street, Athens, Georgia 30602-2501, USA

Ronald W. Kistler
U.S. Geological Survey, 345 Middlefield Road, Menlo Park, California 94025, USA

ABSTRACT

The composite Sunrise Butte pluton, in the central part of the Blue Mountains Province, northeastern Oregon, preserves a record of subduction-related magmatism, arc-arc collision, crustal thickening, and deep-crustal anatexis. The earliest phase of the pluton (Desolation Creek unit) was generated in a subduction zone

Johnson, K., Schwartz, J.J., Žák, J., Verner, K., Barnes, C.G., Walton, C., Wooden, J.L., Wright, J.E., and Kistler, R.W., 2015, Composite Sunrise Butte pluton: Insights into Jurassic–Cretaceous collisional tectonics and magmatism in the Blue Mountains Province, northeastern Oregon, *in* Anderson, T.H., Didenko, A.N., Johnson, C.L., Khanchuk, A.I., and MacDonald, J.H., Jr., eds., Late Jurassic Margin of Laurasia—A Record of Faulting Accommodating Plate Rotation: Geological Society of America Special Paper 513, p. 377–398, doi:10.1130/2015.2513(10).

environment, as the oceanic lithosphere between the Wallowa and Olds Ferry island arcs was consumed. Zircons from this unit yielded a $^{206}Pb/^{238}U$ age of 160.2 ± 2.1 Ma. A magmatic lull ensued during arc-arc collision, after which partial melting at the base of the thickened Wallowa arc crust produced siliceous magma that was emplaced into metasedimentary rocks and serpentinite of the overthrust forearc complex. This magma crystallized to form the bulk of the Sunrise Butte composite pluton (the Sunrise Butte unit; 145.8 ± 2.2 Ma). The heat necessary for crustal anatexis was supplied by coeval mantle-derived magma (the Onion Gulch unit; 147.9 ± 1.8 Ma).

The lull in magmatic activity between 160 and 148 Ma encompasses the timing of arc-arc collision (159–154 Ma), and it is similar to those lulls observed in adjacent areas of the Blue Mountains Province related to the same shortening event. Previous researchers have proposed a tectonic link between the Blue Mountains Province and the Klamath Mountains and northern Sierra Nevada Provinces farther to the south; however, timing of Late Jurassic deformation in the Blue Mountains Province predates the timing of the so-called Nevadan orogeny in the Klamath Mountains. In both the Blue Mountains Province and Klamath Mountains, the onset of deep-crustal partial melting initiated at ca. 148 Ma, suggesting a possible geodynamic link. One possibility is that the Late Jurassic shortening event recorded in the Blue Mountains Province may be a northerly extension of the Nevadan orogeny. Differences in the timing of these events in the Blue Mountains Province and the Klamath–Sierra Nevada Provinces suggest that shortening and deformation were diachronous, progressing from north to south. We envision that Late Jurassic deformation may have collapsed a Gulf of California–style oceanic extensional basin that extended from the Klamath Mountains (e.g., Josephine ophiolite) to the central Blue Mountains Province, and possibly as far north as the North Cascades (i.e., the coeval Ingalls ophiolite).

INTRODUCTION

The Blue Mountains Province of northeastern Oregon and western Idaho (Fig. 1) is generally thought to have been formed by a two-stage process, in which the amalgamation of oceanic- and island-arc terranes was followed by their accretion as a terrane assemblage to the western North American continental margin. Recent studies along the terrane-continent boundary, which is referred to as the Salmon River suture zone, suggest that collision of amalgamated Blue Mountains terranes with the continent occurred around 128 Ma, and that associated deformation continued to ca. 90 Ma (Getty et al., 1993; Snee et al., 1995; Fleck and Criss, 2007; Giorgis et al., 2008; but also see Dorsey and LaMaskin, 2007). Less well known has been the timing of terrane amalgamation. Recent studies suggest that collision of island-arc terranes and the resultant deformation observed in intervening rocks may have occurred from as early as Late Triassic time (Dorsey and LaMaskin, 2007) to as late as the Late Jurassic (Getty et al., 1993; Avé Lallemant, 1995; Schwartz et al., 2010, 2011a).

The juxtaposition of large fragments of lithosphere and their ensuing collision (arc-arc or arc-continent) are commonly marked by an abrupt change in the composition of associated magmatism (Barnes et al., 1992; Tulloch and Kimbrough, 2003), suggestive of a change in the conditions, processes, or source regions of magma generation. For example, in several compressional environments in the western North American Cordillera, long periods of subduction-related, mantle-derived magmatism gave way to a pulse of generally more felsic, crust-derived magmas after contractional orogeny (e.g., Brandon and Smith, 1994; Barnes et al., 1992; Ducea, 2001; Tulloch and Kimbrough, 2003; DeCelles et al., 2009). Tulloch and Kimbrough (2003) described spatially and temporally distinct belts of older plutons with low Sr/Y compositions and younger plutons with high Na_2O, Sr, and Sr/Y, and low Y in New Zealand. Our work in the Blue Mountains Province has demonstrated similar relationships (Johnson et al., 1995, 2007; Schwartz et al., 2011b), commonly within the same pluton.

In this paper, we describe the petrology and geochemistry of the composite Sunrise Butte pluton, which consists in part of both an early low-volume, low-Sr/Y phase and a younger high-volume, high-Sr/Y phase. We present results of U-Pb geochronology (sensitive high-resolution ion microprobe–reverse geometry [SHRIMP-RG]) that confirm the age-composition relationships described elsewhere (Schwartz et al., 2011b, 2014) and document an orogen-wide high-flux event of crust-derived magmas following Late Jurassic shortening. We suggest that the temporal change in magmatism in the Sunrise Butte pluton was related to compressional orogenesis and resultant crustal thickening in the Blue Mountains Province; thus, the ages of high-Sr/Y magmatic rocks in the Blue Mountains Province can be used to constrain the timing of the collision event. We then place these events into

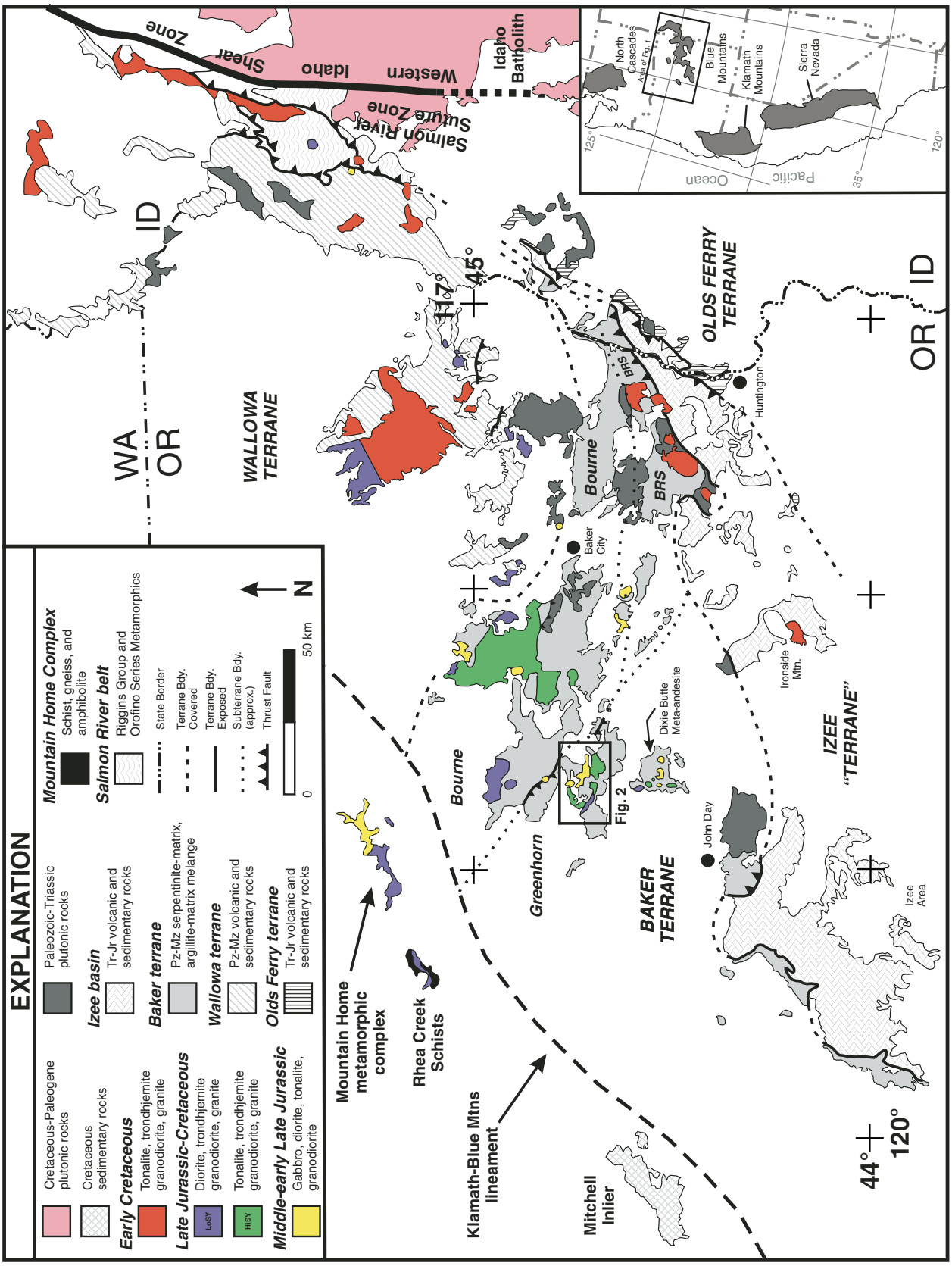

Figure 1. Geologic map of the Blue Mountains Province, northeastern Oregon and westernmost Idaho. Inset shows the position of the Blue Mountains Province relative to other segments of the North American Cordillera. Map is modified from LaMaskin et al. (2009). BRS—Burnt River Schist; Tr—Triassic; Jr—Jurassic; Pz—Paleozoic, Mz—Mesozoic; WA—Washington; OR—Oregon; ID—Idaho.

a regional context and discuss possible links to deformational and magmatic events in other parts of the North American Cordillera.

GEOLOGICAL FRAMEWORK

The Blue Mountains Province is an assemblage of at least three oceanic- and island-arc terranes (Fig. 1). They are, from generally northwest to southeast, the Wallowa island-arc terrane, the Baker forearc and accretionary-complex terrane, and the Olds Ferry island-arc terrane. The Izee "terrane" is not a separate lithotectonic unit but consists of an overlap sequence of Early to Late Jurassic clastic sedimentary rocks that lie unconformably on the older terranes (Dorsey and LaMaskin, 2007). The Baker terrane is further divided into two subterranes (Ferns and Brooks, 1995), which include an accretionary-wedge complex (Bourne subterrane) and the forearc, presumably of the Olds Ferry arc (Greenhorn subterrane; Fig. 1). Collision of the island arcs resulted in thrusting of the Bourne subterrane over the Wallowa terrane and intercalation of tectonic slices of both terranes at the southern margin of the Wallowa arc (Schwartz et al., 2010). Schwartz et al. (2011a) determined that arc-arc collision occurred between 159 and 154 Ma.

The eastern ends of the Blue Mountains Province terranes extend into westernmost Idaho, where they abut the Western Idaho shear zone (Fig. 1). The amalgamated terrane assemblage underwent large post-Cretaceous clockwise rotation (for discussion, see Wilson and Cox, 1980; Hillhouse et al., 1982; Housen, and Dorsey, 2005). When the Blue Mountains Province is restored to its prerotation configuration, the terrane axes assume a roughly N–S orientation, parallel to the continental margin as defined by the 0.706 initial $^{87}Sr/^{86}Sr$ isopleth of Armstrong et al. (1977).

An examination of the existing Pb/U ages for plutons and batholiths in the Blue Mountains Province demonstrates that magmatism occurred in several distinct episodes throughout Late Jurassic–Early Cretaceous time (Walker, 1989; Manduca et al., 1993; Lee, 2004; McLelland and Oldow, 2007; Snee et al., 2007; Unruh et al., 2008; Schwartz et al., 2010, 2011a, 2011b). The first of these episodes is marked by several 162–154 Ma plutons that were emplaced slightly before and during collision of the Wallowa and Olds Ferry arcs (from 159 to 154 Ma; Schwartz et al., 2011b). These plutons consist of rocks that have low Sr/Y ratios, and they are mostly restricted geographically to the western part of the Blue Mountains Province. Following arc-arc collision, mixtures of plutons having both low-Sr/Y and high-Sr/Y compositions were emplaced between 148 and 141 Ma, with high-Sr/Y rocks primarily restricted to the Baker terrane (Schwartz et al., 2011b). A similar pattern is seen during Early Cretaceous time, 134–130 Ma, where predominantly low-Sr/Y plutons were emplaced shortly before collision of the Blue Mountains Province with the North American continent (128 ± 3 Ma; Getty et al., 1993), followed by low-Sr/Y and high-Sr/Y plutons from 124 to 111 Ma (Johnson et al., 1997; Lee, 2004; Snee et al., 2007).

Sunrise Butte Pluton

The Sunrise Butte pluton is located within the belt of Late Jurassic–Early Cretaceous plutons at the western end of the Blue Mountains Province (Fig. 1). Sunrise Butte magmas were emplaced into the Greenhorn subterrane of the Baker terrane. The northern part of the pluton is composed of pyroxene-bearing hornblende biotite quartz diorite and tonalite of the Desolation Creek unit (Fig. 2). A small body of two-pyroxene diorite (the Onion Gulch unit) crops out along the southwestern margin of the Sunrise Butte pluton. The bulk of the exposed pluton consists of hornblende biotite tonalite and granodiorite of the Sunrise Butte unit.

Chert-rich graphitic metasedimentary rocks of the Badger Creek unit (in the Greenhorn subterrane of Ferns and Brooks, 1995) and subordinate metagabbro and serpentinized ultramafic rocks occur along the southern margin of the pluton and as a <1-km-wide septum between the Sunrise Butte and Desolation Creek units (Fig. 2; Brooks et al., 1983; Ferns et al., 1984; Evans, 1989). Xenoliths of purported Badger Creek metasedimentary rocks occur throughout the Sunrise Butte pluton (Fig. 3A), especially adjacent to the pluton–wall-rock contacts. Mafic magmatic enclaves occur throughout the pluton, most of which have thin (<1-cm-wide), fine-grained chilled margins. Some enclaves contain xenoliths of metasedimentary rock (Fig. 3B). Mafic dikes coeval with Sunrise Butte magmatism were not observed in any intrusions comprising the composite Sunrise Butte pluton.

RESULTS

Petrography

One sample from each of the three plutonic units was analyzed for mineral chemistry. Most rocks from the Sunrise Butte, Desolation Creek, and Onion Gulch units are coarse grained and hypidiomorphic granular. Some samples show a seriate grain-size distribution. Apatite, sphene, and zircon are common accessory phases in all units. Rocks from the Sunrise Butte unit contain plagioclase, quartz, green magnesiohornblende (Leake, 1978), and brown biotite (with average MgO/[MgO + FeO] = 0.532 ± 0.018), plus lesser amounts of magnetite and interstitial K-feldspar. Pyroxene was not observed in these rocks. Onion Gulch rocks contain variable amounts of augite ($En_{37–45}$-$Fs_{15–25}$-$Wo_{30–46}$) and orthopyroxene ($En_{53–58}$-$Fs_{39–45}$-$Wo_{1–7}$), in addition to plagioclase, quartz, green magnesio-hornblende, and brown biotite (average MgO/[MgO + FeO] = 0.554 ± 0.013); in fact, pyroxenes are the dominant ferromagnesian phases in a large portion of the Onion Gulch unit. Most Desolation Creek rocks are similar in mineralogy to Sunrise Butte rocks, but some contain augite, weakly pleochroic light-brown hornblende, and reddish-brown biotite (average MgO/[MgO + FeO] = 0.494 ± 0.014). Total Al in the Desolation Creek biotites averages 2.560 ± 0.093 atoms p.f.u., which

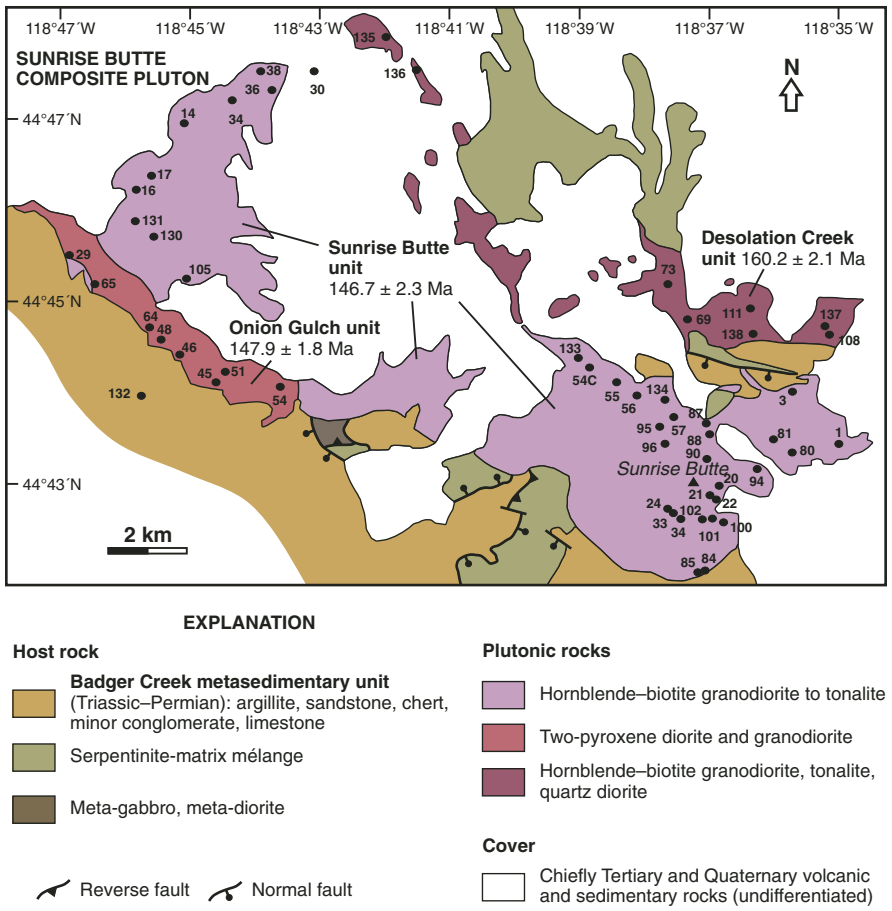

Figure 2. Simplified geologic map of the Sunrise Butte pluton, showing the localities of samples used in this study. Map is modified from geologic maps by Brooks et al. (1983), Ferns et al. (1984), and Evans (1989).

is higher than in biotites from the Sunrise Butte unit (Al_{total} = 2.342 ± 0.111 atoms p.f.u.). Augite occurs as cores within either (1) the light-brown hornblende, or (2) colorless actinolitic hornblende and actinolite (Leake, 1978), which is in turn rimmed with the light-brown hornblende. Interstitial quartz and poikilitic K-feldspar are common. Minor amounts of tourmaline were observed in some Desolation Creek rocks. At least one sample from the Desolation Creek unit exhibits flattened quartz and sutured quartz grain boundaries, characteristic of regime II quartz microstructures (Fig. 3C; Hirth and Tullis, 1992); no such deformation was observed in the Sunrise Butte unit or the Onion Gulch unit rocks. Aluminum-in-hornblende barometry (Anderson and Smith, 1995) suggests that the Sunrise Butte composite pluton was emplaced at pressures less than 2 kbar.

Magmatic enclaves throughout the Sunrise Butte pluton are generally medium grained and slightly porphyritic with phenocrysts of hornblende and plagioclase. Biotite is a common ferromagnesian phase, and the biotite:hornblende ratio is visibly greater in enclaves from the Desolation Creek unit than in those from the Sunrise Butte unit. In several of the enclaves, hornblende was rimmed entirely with fine-grained biotite. Poikilitic K-feldspar is rare. Accessory apatite is acicular, with aspect ratios generally greater than 10:1.

Tonalitic and granodioritic dikes in the Sunrise Butte pluton are commonly porphyritic, with phenocrysts of plagioclase, rounded quartz, and biotite ± hornblende in a fine-grained groundmass of plagioclase, quartz, and biotite. Granitic dikes have a seriate grain-size distribution and contain biotite as the only ferromagnesian phase. Muscovite and spessartine-rich garnet are common.

Xenoliths correspond in mineralogy to the adjacent wall rocks and consist of variably serpentinized peridotite, medium-grained pyroxene hornfels, and fine-grained biotite + plagioclase + quartz schists. Some hornfels and schist samples retain original sedimentary layering.

Zircon Geochronology

A tonalite (SB-137) from the Desolation Creek pluton yielded 12 concordant SHRIMP-RG spot analyses that give a combined error-weighted average $^{206}Pb/^{238}U$ age of 159.5 ± 2.4 Ma (mean square of weighted deviates [MSWD] = 0.5; Fig. 4A; Table 1). One analysis is younger than the rest (152.9 Ma) and may represent slight Pb loss. Excluding this analysis as an outlier, the remaining 11 spot analyses yield a statistically identical error-weighted average $^{206}Pb/^{238}U$ age of 160.2 ± 2.1 Ma (MSWD = 0.5)

with a slightly lower 2σ error. We interpret this age as the best estimate of the crystallization age; however, the 159.5 ± 2.4 Ma age is also considered viable.

A quartz diorite (JZ-33) from the Onion Gulch pluton yielded 10 concordant spot analyses. The error-weighted average age of all spot analyses yields a $^{206}Pb/^{238}U$ age of 147.9 ± 1.8 Ma (MSWD = 0.9; Fig. 4B).

A granodiorite (SB-1) from the Sunrise Butte pluton yielded nine concordant SHRIMP-RG spot analyses and one slightly discordant analysis with $^{206}Pb/^{238}U$ ages ranging from 150 to 114 Ma. The error-weighted average $^{206}Pb/^{238}U$ age of all spot analyses is 137 ± 10 Ma (MSWD = 18). The large MSWD of these data and their large overdispersion of dates (36 m.y.) suggest a component of nonanalytical scatter in the data. The majority of the spot analyses (n = 7) define an age distribution with $^{206}Pb/^{238}U$ ages ranging from 150 to 143 Ma, whereas three spot analyses (including the discordant spot) yield younger ages ranging from 114 to 139 Ma. We interpret the three younger ages as likely reflecting postcrystallization Pb loss. Excluding these analyses, the error-weighted average $^{206}Pb/^{238}U$ age of the remaining seven spot analyses is 145.8 ± 2.2 Ma (MSWD = 1.9; Fig. 4C).

The Pb/U ages demonstrate that construction of the Sunrise Butte composite pluton began in the Late Jurassic with emplacement of the low-Sr/Y Desolation Creek magma. Following an ~12 m.y. lull, magmatism recommenced during Early Cretaceous time with simultaneous emplacement of both low-Sr/Y (Onion Gulch unit) and high-Sr/Y (Sunrise Butte unit) magmas. Similar age-composition relationships have been observed in other intrusive bodies in the Baker terrane (Schwartz et al., 2011b, 2014).

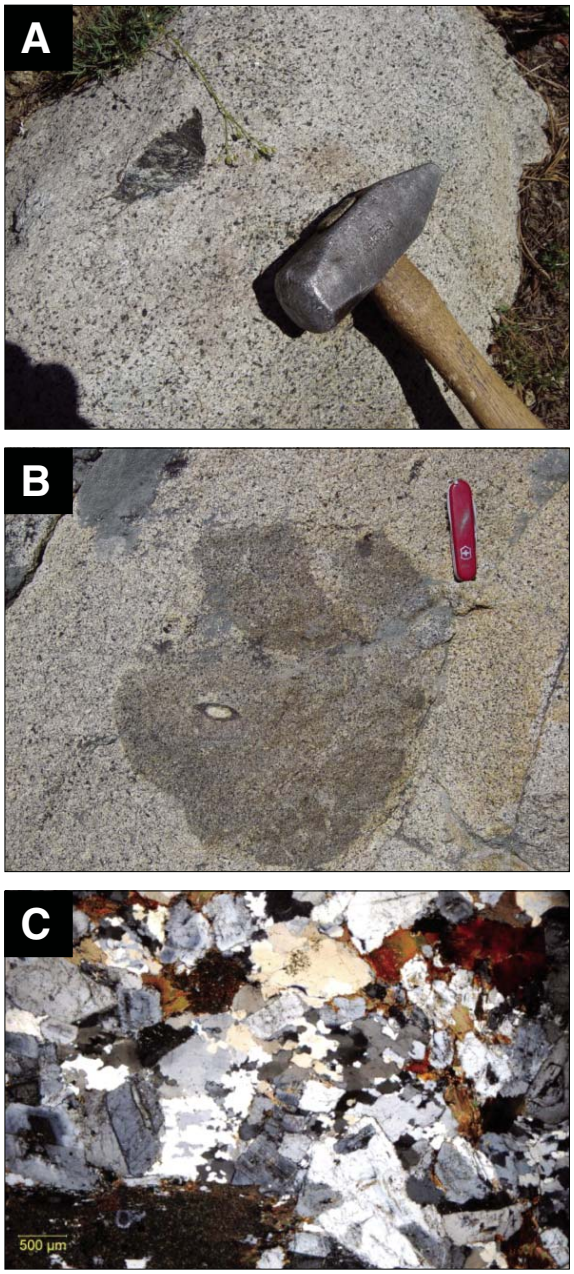

Figure 3. Photographs and photomicrographs from the Sunrise Butte pluton. (A) Xenolith of purported Badger Creek metasedimentary rock in the Sunrise Butte unit. (B) Mafic magmatic enclave with a metasedimentary xenolith. Note the reaction rim around the xenolith. (C) Photomicrograph of flattened quartz and sutured quartz boundaries in tonalite of the Desolation Creek unit.

Whole-Rock Major and Trace Elements

Whole-rock major- and trace-element compositions of representative samples are in Table 2, and data for all samples can be found in Supplementary Table DR1.[1] Samples from the composite Sunrise Butte pluton span a range of SiO_2 contents from 55 to 76 wt% (Fig. 5). The greatest range in SiO_2 contents is observed in the Sunrise Butte unit (from ~59 to 73 wt%); the samples with the lowest SiO_2 contents are from the margins of the pluton. Rocks of the Desolation Creek and Onion Gulch units all have SiO_2 contents below 67 wt%. The composite Sunrise Butte pluton as a whole exhibits an increase in the aluminum saturation index [A/CNK = $Al_2O_3/(CaO + Na_2O + K_2O)$ in moles] with increasing SiO_2. In general, samples with >70 wt% SiO_2 are mildly peraluminous (A/CNK = 1.0–1.1), whereas those with lower SiO_2 contents are metaluminous (A/CNK < 1.0). Enclaves exhibit a narrow range in SiO_2 content, from 55 to 59 wt%. The garnet-bearing aplitic dike has an SiO_2 content >75 wt% and is strongly peraluminous (A/CNK = 1.12). According to the classification scheme of Frost et al. (2001), all samples from the Sunrise Butte, Desolation Creek, and Onion Gulch units are "magnesian" and "calcic." Most of the enclave samples plot in the "calc-alkalic" field, and the granitic dike is classified as "ferroan" and "calc-alkalic."

[1]GSA Data Repository Item 2015332, Table DR1: Whole rock major and trace element compositions; Table DR2: Zircon Lu-Hf isotope data; and Figure DR1, is available at www.geosociety.org/pubs/ft2015.htm, or on request from editing@geosociety.org or Documents Secretary, GSA, P.O. Box 9140, Boulder, CO 80301-9140, USA.

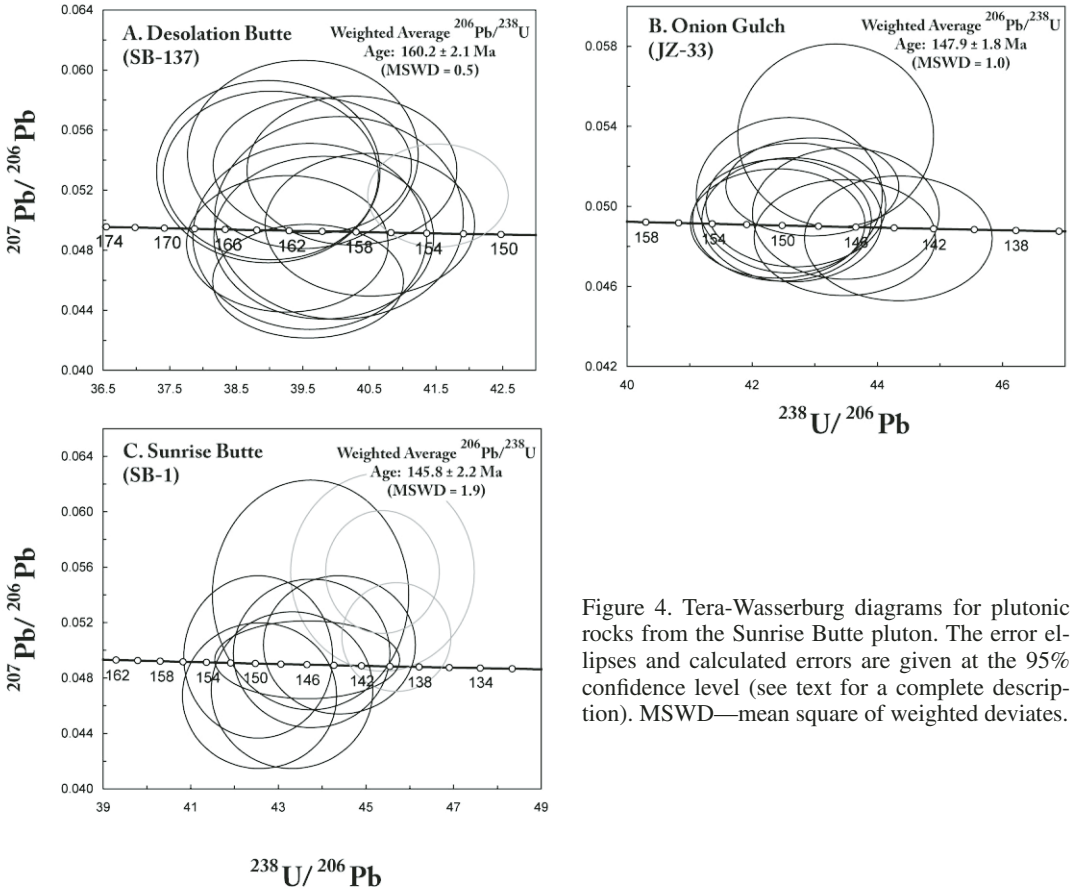

Figure 4. Tera-Wasserburg diagrams for plutonic rocks from the Sunrise Butte pluton. The error ellipses and calculated errors are given at the 95% confidence level (see text for a complete description). MSWD—mean square of weighted deviates.

Most tonalitic and granodioritic rocks have >15 wt% Al_2O_3 at the 70 wt% SiO_2 level, which would classify them as "high-alumina" (Barker, 1979; Drummond and Defant, 1990).

Rocks from the Sunrise Butte, Desolation Creek, and Onion Gulch units exhibit collinear decreases in TiO_2, Fe^T (total Fe as Fe_2O_3), MnO, MgO, CaO, and V with increasing SiO_2 contents, whereas they show parallel, but not collinear, decreases in P_2O_5, Sc, Y, and Co. All three units display an increase in K_2O, Rb, and Ba contents with increasing SiO_2, and a decrease in Sr. In comparison to the Sunrise Butte unit, rocks from the Desolation Creek unit are higher in Sc, Y, Co, Hf, and Th and trend toward higher Nb and Zr with increasing SiO_2. Rocks from the Sunrise Butte and Onion Gulch units have ~400–800 ppm Sr, whereas those from the Desolation Creek unit have <200 ppm (Fig. 5E). In addition to Sr, Desolation Creek rocks are also lower in Na_2O and P_2O_5. There is considerable scatter in Al_2O_3, Zr, Nb, Cs, Th, and Hf abundances.

Chondrite-normalized (Sun and McDonough, 1989) rare earth element (REE) patterns distinguish rocks of the Sunrise Butte, Desolation Creek, and Onion Gulch units (Fig. 6). All REE patterns have negative slopes, but rocks from the Sunrise Butte unit (Fig. 6C) are generally more fractionated (La_N/Yb_N = 10.5–14.6; Yb_N = 3.9–5.3) than those from the Desolation Creek (La_N/Yb_N = 4.5–5.6; Yb_N = 12.4–16.6) and Onion Gulch (La_N/Yb_N = 6.4–9.7; Yb_N = 9.4–11.2) units (Figs. 6A and 6B, respectively). The lowest SiO_2 sample from the Sunrise Butte unit (with 59.21 wt% SiO_2) is enriched in ΣREE abundances (La_N/Yb_N = 8.5 and Yb_N = 8.8). Europium anomalies are small to absent in Sunrise Butte (Eu/Eu* = 0.88–1.12) and Onion Gulch rocks (Eu/Eu* = 0.83–0.97), but they are more pronounced in Desolation Creek rocks (Eu/Eu* = 0.69–0.76). Enclave samples have La_N/Yb_N = 5.5–7.5 and Yb_N = 11.2–16.5, with pronounced negative europium anomalies (Eu/Eu* = 0.60–0.74; Fig. 6D).

Sr, Nd, and O Isotopes

Samples from all three plutons and a granitic dike were analyzed for Sr and Nd isotopes. Several additional samples, including magmatic enclaves, were also analyzed for O isotopes. Only one sample from the Onion Gulch unit was analyzed. Initial $^{87}Sr/^{86}Sr$ and epsilon Nd (ε_{Nd}) values for each unit were calculated for their respective $^{206}Pb/^{238}U$ ages (Table 2; see previous). Initial

TABLE 1. U-Pb SENSITIVE HIGH-RESOLUTION ION MICROPROBE (SHRIMP) ISOTOPIC ANALYSES AND AGES

	Concentrations				Atomic ratios†							Age (Ma)		
Grain	U (ppm)	Th (ppm)	Th/U	Pb†§ (ppm)	*f*206# (%)	$^{238}U/^{206}Pb$**	% err (1σ)	$^{207}Pb/^{206}Pb$**	% err (1σ)	$^{206}Pb/^{238}U$††	err abs (1σ)	$^{206}Pb/^{238}U$§§	Err abs (1σ)	Weighted average age (2σ)
Desolation Butte tonalite														
SB-137-1	84.58	39.54	0.47	1.84	0.64	39.50	1.8	0.0544	4.7	0.0252	0.0005	160.1	2.9	160.2 ± 2.1
SB-137-2	81.42	45.22	0.56	1.77	–0.04	39.60	1.8	0.0489	5.2	0.0253	0.0005	160.8	2.9	(MSWD = 0.5)##
SB-137-3	146.06	69.31	0.47	3.20	–0.11	39.27	1.6	0.0484	3.8	0.0255	0.0004	162.3	2.6	
~~SB-137-4~~	~~111.94~~	~~63.08~~	~~0.56~~	~~2.32~~	~~0.32~~	~~41.53~~	~~1.7~~	~~0.0516~~	~~4.4~~	~~0.0240~~	~~0.0004~~	~~152.9~~	~~2.6~~	
SB-137-5	137.81	82.73	0.60	2.94	0.52	40.24	1.6	0.0533	3.8	0.0247	0.0004	157.4	2.5	
SB-137-6	106.71	59.07	0.55	2.35	0.46	39.02	1.7	0.0530	4.3	0.0255	0.0004	162.4	2.8	
SB-137-7	98.78	54.79	0.55	2.18	0.49	38.98	1.8	0.0532	4.7	0.0255	0.0005	162.5	2.9	
SB-137-8	216.76	109.17	0.50	4.70	–0.42	39.58	1.5	0.0459	3.4	0.0254	0.0004	161.5	2.4	
SB-137-9	107.92	60.01	0.56	2.33	–0.05	39.81	1.7	0.0488	4.5	0.0251	0.0004	160.0	2.7	
SB-137-10	133.82	71.86	0.54	2.84	0.06	40.51	1.6	0.0497	3.9	0.0247	0.0004	157.1	2.5	
SB-137-11	166.03	95.78	0.58	3.60	0.55	39.64	1.5	0.0536	3.5	0.0251	0.0004	159.7	2.5	
SB-137-12	70.88	23.48	0.33	1.52	0.12	40.05	1.9	0.0502	5.5	0.0249	0.0005	158.8	3.1	
Onion Gulch tonalite														
JZ-33-1	549.36	268.73	0.49	10.99	0.25	42.96	1.3	0.0510	2.0	0.0232	0.0003	148.0	1.9	147.9 ± 1.8
JZ-33-2	353.52	246.92	0.70	7.12	0.04	42.63	1.4	0.0493	2.6	0.0234	0.0003	149.4	2.1	(MSWD = 0.9)
JZ-33-3	270.31	166.77	0.62	5.45	0.19	42.59	1.4	0.0506	3.1	0.0234	0.0003	149.3	2.1	
JZ-33-4	376.35	207.18	0.55	7.44	–0.07	43.48	1.4	0.0484	2.4	0.0230	0.0003	146.7	2.0	
JZ-33-5	351.77	214.18	0.61	7.12	0.03	42.47	1.4	0.0493	2.5	0.0235	0.0003	150.0	2.1	
JZ-33-6	353.90	240.19	0.68	6.86	–0.06	44.33	1.4	0.0484	2.6	0.0226	0.0003	143.9	2.0	
JZ-33-7	319.01	182.20	0.57	6.30	0.08	43.50	1.4	0.0496	2.7	0.0230	0.0003	146.4	2.1	
JZ-33-8	448.13	227.70	0.51	9.08	0.01	42.41	1.3	0.0491	2.3	0.0236	0.0003	150.2	2.0	
JZ-33-9	219.20	130.13	0.59	4.35	0.57	43.33	1.5	0.0535	3.5	0.0229	0.0003	146.2	2.2	
JZ-33-10	364.04	206.95	0.57	7.32	0.13	42.70	1.4	0.0501	2.5	0.0234	0.0003	149.0	2.0	
Sunrise Butte tonalite														
~~SB-1-1~~	~~77.51~~	~~22.78~~	~~0.29~~	~~1.47~~	~~0.86~~	~~45.38~~	~~1.9~~	~~0.0557~~	~~5.3~~	~~0.0218~~	~~0.0004~~	~~139.3~~	~~2.7~~	145.8 ± 2.2
SB-1-2	54.18	18.57	0.34	1.06	0.64	43.73	2.1	0.0540	6.3	0.0227	0.0005	144.8	3.1	(MSWD = 1.9)
SB-1-3	442.53	152.06	0.34	8.71	0.04	43.66	2.0	0.0493	2.3	0.0229	0.0005	145.9	2.9	
SB-1-4	113.20	31.65	0.28	2.28	–0.29	42.57	1.7	0.0467	4.6	0.0236	0.0004	150.1	2.5	
SB-1-5	130.05	47.24	0.36	2.63	0.06	42.54	1.6	0.0495	4.8	0.0235	0.0004	149.7	2.5	
SB-1-6	117.72	42.56	0.36	2.31	0.10	43.76	1.7	0.0498	4.4	0.0228	0.0004	145.5	2.4	
SB-1-7	144.20	47.78	0.33	2.79	0.19	44.39	1.6	0.0504	4.0	0.0225	0.0004	143.3	2.3	
~~SB-1-8~~	~~163.88~~	~~118.71~~	~~0.72~~	~~2.55~~	~~1.51~~	~~55.22~~	~~1.6~~	~~0.0603~~	~~5.6~~	~~0.0178~~	~~0.0003~~	~~114.0~~	~~1.9~~	
SB-1-9	97.90	22.62	0.23	1.94	–0.23	43.31	1.7	0.0471	4.9	0.0231	0.0004	147.5	2.6	
~~SB-1-10~~	~~89.68~~	~~25.62~~	~~0.29~~	~~1.69~~	~~0.27~~	~~45.70~~	~~1.8~~	~~0.0510~~	~~5.1~~	~~0.0218~~	~~0.0004~~	~~139.2~~	~~2.5~~	

†Errors are reported at 1σ level and refer to last digits.
§Radiogenic ^{206}Pb.
#Fraction of total ^{206}Pb that is common ^{206}Pb.
**Uncorrected ratios.
††^{207}Pb corrected ratios using age-appropriate Pb isotopic composition of Stacey and Kramers (1975).
§§^{207}Pb corrected age; spot analyses with strikethrough were excluded in age calculation due to open system behavior and/or analytical problems.
##MSWD—mean square of weighted deviates.

$^{87}Sr/^{86}Sr$ values for Desolation Creek rocks (0.7042–0.7047) overlap with those of the Sunrise Butte rocks (0.7041–0.7045), whereas the Onion Gulch sample has a slightly more primitive initial $^{87}Sr/^{86}Sr$ value of 0.7040. The granitic dike sample had a more-evolved ratio of 0.7055.

Samples from the Sunrise Butte unit have initial ε_{Nd} values that range from +1.4 to +2.5; a sample from the Desolation Creek unit has a similar value of +1.5, and the Onion Gulch sample yielded a slightly more radiogenic ε_{Nd} value of +3.0. The granitic dike sample has an ε_{Nd} value of –2.1 (Fig. 7A).

Rocks from the Sunrise Butte unit have $\delta^{18}O$ values between +10.2‰ and +12.2‰; one outlier has a value of +4.1‰. Two Desolation Creek samples have $\delta^{18}O$ values of +10.2‰ and +11.1‰, whereas a third sample has a very low $\delta^{18}O$ value of –1.3‰. The Onion Gulch sample yielded a $\delta^{18}O$ value of +9.0‰. Two magmatic enclaves within the Sunrise Butte unit have $\delta^{18}O$ values of +10.3‰ and +10.7‰; an enclave within the Desolation Creek unit has a low value of –1.9‰. The granitic dike yielded a $\delta^{18}O$ value of +14.5‰. Although the three samples with anomalously low $\delta^{18}O$ values (SB-105, SB-111, and SB-70B) exhibited only minor alteration (sericitization of plagioclase, chloritization of biotite), it is clear that these values are not magmatic and therefore probably reflect postemplacement alteration.

TABLE 2. REPRESENTATIVE WHOLE-ROCK COMPOSITIONS

	Desolation Creek				Onion Gulch			Sunrise Butte									Enclaves			Dikes		
	SB-73	SB-69A	SB-111	SB-109	SB-15	SB-64A	SB-51	SB-54C	SB-55	SB-100	SB-20A	SB-90	SB-3	SB-1	SB-34W	SB-16	SB-70B	SB-37	SB-54E	SB-21B	SB-33	SB-94B
SiO_2	66.14	58.51	63.73	63.67	57.99	62.29	56.18	68.57	59.21	71.37	69.81	71.20	71.76	72.28	71.21	68.32	58.77	55.01	57.01	75.49	70.85	69.01
TiO_2	0.63	0.91	0.73	0.72	0.87	0.73	0.98	0.46	0.91	0.31	0.35	0.27	0.28	0.23	0.29	0.49	0.72	0.81	0.97	0.06	0.34	0.43
Al_2O_3	15.46	15.94	14.68	15.61	15.70	15.67	15.95	15.34	16.94	15.39	15.26	15.34	15.25	14.95	15.90	14.97	14.81	13.90	16.31	13.87	16.01	16.20
Fe_2O_3	4.86	7.48	5.48	5.77	7.31	5.51	8.26	3.05	6.69	2.23	2.36	2.01	2.08	1.88	2.20	3.49	6.81	9.17	7.15	0.89	2.00	2.83
MnO	0.09	0.14	0.11	0.11	0.14	0.10	0.16	0.06	0.12	0.05	0.06	0.05	0.05	0.05	0.06	0.08	0.13	0.31	0.21	0.05	0.05	0.04
MgO	2.69	5.02	3.36	3.23	4.53	3.19	5.20	1.62	3.96	0.89	0.95	0.77	0.78	0.64	0.91	1.84	5.60	7.19	4.40	0.10	0.83	1.16
CaO	5.08	8.03	5.54	5.80	6.74	5.75	8.34	4.09	7.14	3.50	3.52	3.22	3.27	2.93	3.57	3.94	7.25	7.23	6.30	1.02	3.48	4.05
Na_2O	2.93	2.83	3.06	3.04	3.07	3.26	2.83	3.94	3.68	4.48	4.22	4.31	4.22	4.35	4.33	3.66	3.28	3.44	4.13	4.06	4.53	4.40
K_2O	2.28	0.72	1.99	1.85	1.95	2.26	1.42	1.68	1.01	1.57	1.69	1.54	1.67	1.51	1.48	2.34	1.64	1.52	1.51	3.57	1.54	1.07
P_2O_5	0.11	0.15	0.13	0.15	0.24	0.20	0.25	0.15	0.28	0.10	0.11	0.08	0.08	0.08	0.09	0.14	0.14	0.25	0.27	0.04	0.11	0.14
LOI	0.56	0.70	0.84	0.55	0.87	0.35	0.21	0.37	0.56	0.37	0.41	0.57		0.45	0.58	0.53	0.89	1.18	0.81	0.21	0.48	0.46
Total	100.83	100.43	99.65	100.51	99.40	99.31	99.77	99.33	100.50	100.27	98.73	99.36	99.44	99.36	100.62	99.80	100.04	100.00	99.07	99.36	100.22	99.80
Sc	14.4	28.9	18.9	18.2	21.9	16.0	25.1	6.0	15.7	3.8	4.4	3.2	3.5	2.9	4.3	7.0	21.6	26.2	17.7	2.7	3.2	4.4
V	80	164	106	118	162	125	196	64	137	30	32	26	25	16	29	64	132	161	134	2	28	49
Zn	49	70	62	48	81	73	88	50		44	52	43	37	38	46	65		212	138	19	42	40
Nb	13	6	11	10	9	9	6	5	7	5	5	5	6	6	6	9	9	5	12	14	6	5
Sr	175	203	170	188	570	559	584	656	779	663	533	546	518	497	637	521	180	387	566	143	650	658
Ba	841	343	771	662	538	1160	746	1095	613	1084	891	828	992	1088	946	1021	547	883	863	1454	1130	867
Zr	175	115	174	174	208	170	105	107	103	96	98	99	91	97	105	94	145	86	113	44	113	111
Y	26.7	30.6	34.5	30.5	22.3	20.2	22.1	7.7	16.4	6.9	9.4	8.8	6.9	7.1	9.4	10.1	37.8	36.1	24.6	14.7	8.6	8.4
Rb	70	21	63	55	46	55	30	35	29	38	39	41	39	40	35	55		35	35	122	37	23
Co	13.80		17.80	17.60	19.22	15.30	22.28	7.82	16.70	3.52	3.50	2.64	2.82	2.07	3.33	7.97		23.59	19.29	0.40	3.32	5.77
Sb	0.17		0.48	0.22	0.30	0.18	0.21	0.12	0.20	0.08	0.04	0.08	0.09	0.10		0.12		0.12	0.17	0.27		
Cs	1.89		4.83	2.62	1.81	1.81	1.40	0.87	1.20	1.27	0.75	2.85	1.02	1.56	1.38	1.05		0.74	0.85	3.50	0.94	0.82
Hf	4.78		4.73	4.83	4.11	4.36	3.44	2.77	3.10	2.52	2.66	2.75	2.59	2.54	3.14	3.01		3.27	3.27	1.64	2.95	2.77
Ta	0.69		0.68	0.65	0.60	0.58	0.31	0.29	0.40	0.23	0.29	0.37	0.24	0.26	0.34	0.53		0.35	0.36	0.67	0.28	0.24
Th	5.33		4.87	4.49	10.00	4.05	3.33	2.76	2.14	1.97	3.07	2.58	2.61	2.25	2.56	6.47		2.06	2.75	4.27	2.16	1.64
La	16.50		20.20	16.30	21.80	21.60	17.00	15.70	17.80	11.90	14.30	12.50	11.90	10.50	14.70	17.50		21.60	19.90	12.30	8.60	10.80
Ce	31.60		36.50	34.80	44.60	46.30	35.60	27.30	35.20	21.60	23.70	22.70	22.60	19.40	27.80	31.20		52.90	50.10	20.80	17.00	21.90
Nd	15.40		19.20	17.60	20.90	22.50	17.30	12.70	19.00	10.30	10.50	11.50	9.10	7.70	13.30	16.20		32.00	30.00	9.70	9.20	12.30
Sm	3.68		4.39	4.12	4.47	4.31	4.12	2.72	3.76	2.19	2.48	2.13	1.77	1.44	2.08	2.49		8.64	6.66	1.80	1.81	2.43
Eu	0.93		1.02	0.98	1.16	1.12	1.27	0.71	1.25	0.57	0.63	0.58	0.59	0.49	0.65	0.74		1.58	1.51	0.25	0.65	0.77
Tb	0.61		0.76	0.73	0.61	0.55	0.59	0.24	0.56	0.20	0.27	0.24	0.21	0.18	0.30	0.29		1.14	0.89	0.29	0.21	0.28
Yb	2.10		2.83	2.58	1.70	1.60	1.90	0.78	1.50	0.66	0.86	0.85	0.68	0.64	0.90	0.86		2.80	1.90	1.20	0.77	0.62
Lu	0.33		0.39	0.37	0.23	0.21	0.30	0.09	0.20	0.08	0.12	0.10	0.11	0.09	0.13	0.13		0.41	0.28	0.16	0.10	0.11
Sr(i)	0.704725		0.704191	0.704382		0.703958		0.704197		0.704166	0.704288	0.704201		0.704486		0.704116				0.705534	0.704469	
Nd(i)	0.512510					0.512601		0.512542		0.512523						0.512575				0.512342		
ε_{Nd}	1.5					3.0		1.8		1.4						2.5				–2.1		
$\delta^{18}O$ (‰)	11.1		–1.3	10.2		9.0		11.2		10.7	11.2	11.7		12.2		10.7	–1.9	10.7	10.3	14.5	10.9	

Notes: Oxides are in weight percent, and trace elements are in parts per million (ppm); Sr(i) and Nd(i) are the initial $^{87}Sr/^{86}Sr$ and $^{143}Nd/^{144}Nd$ values, respectively, calculated for each sample's U-Pb age (see Table 1); LOI—loss on ignition.

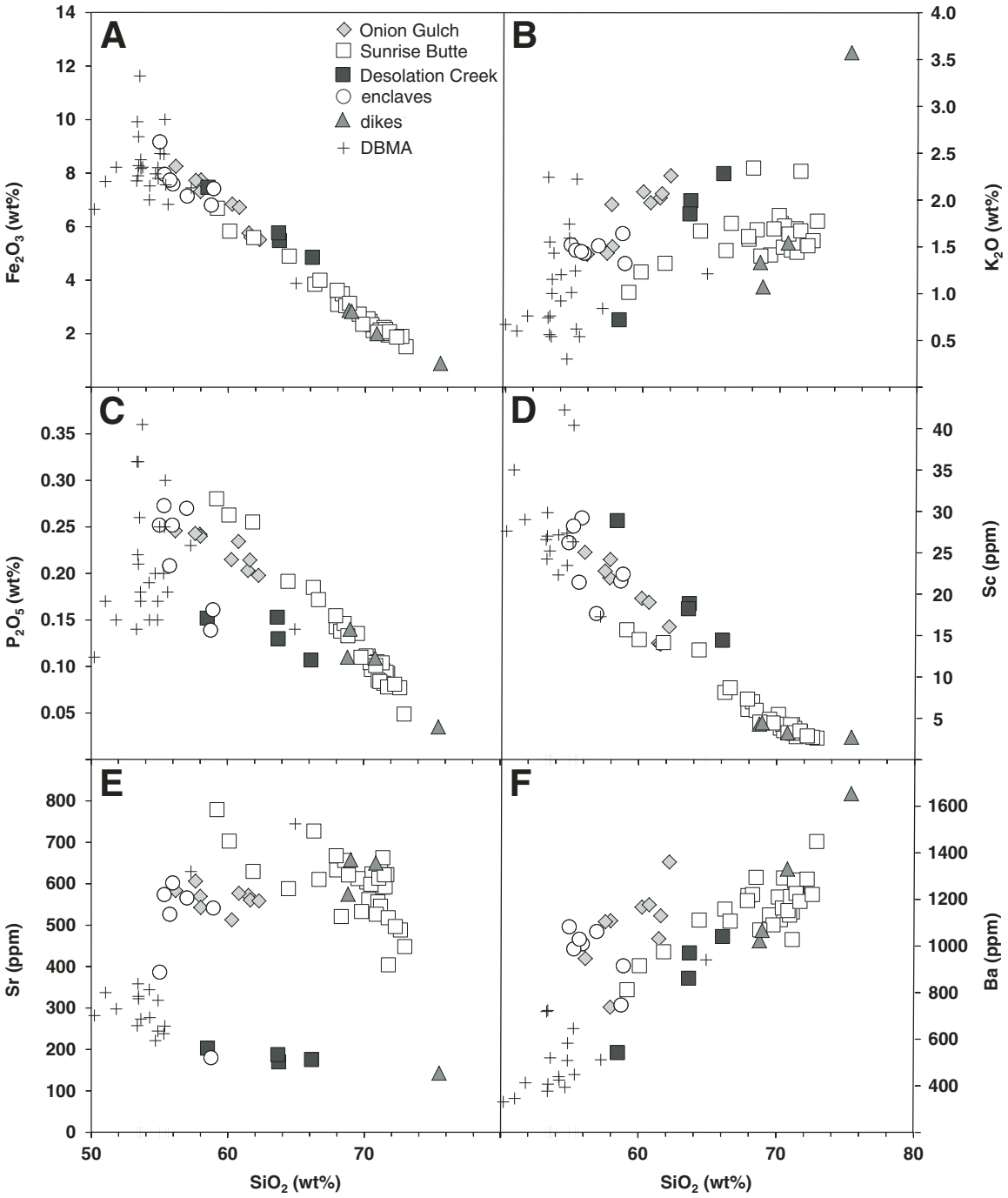

Figure 5. Harker diagrams showing variations in selected major and trace elements with SiO_2. Additional data for the Dixie Butte meta-andesite (DBMA) are from Schwartz et al. (2011b). See text for discussion of Dixie Butte meta-andesite data.

In general, samples from the Sunrise Butte and Desolation Creek units show an increase in initial $^{87}Sr/^{86}Sr$ and $\delta^{18}O$ (excluding those samples with anomalously low $\delta^{18}O$ values) with increasing SiO_2 and A/CNK (Figs. 7B and 7C). Among the samples from the Sunrise Butte unit, a negative correlation exists between ε_{Nd} and both SiO_2 and A/CNK.

Zircon Lu-Hf Isotope Geochemistry

Lu-Hf isotopic data were collected from 53 zircons to evaluate possible changes in sources and petrogenetic processes through time (cf. Fig. 8; Supplementary Table DR2 [see footnote 1]). Magmatic zircons from the older, Desolation Creek pluton

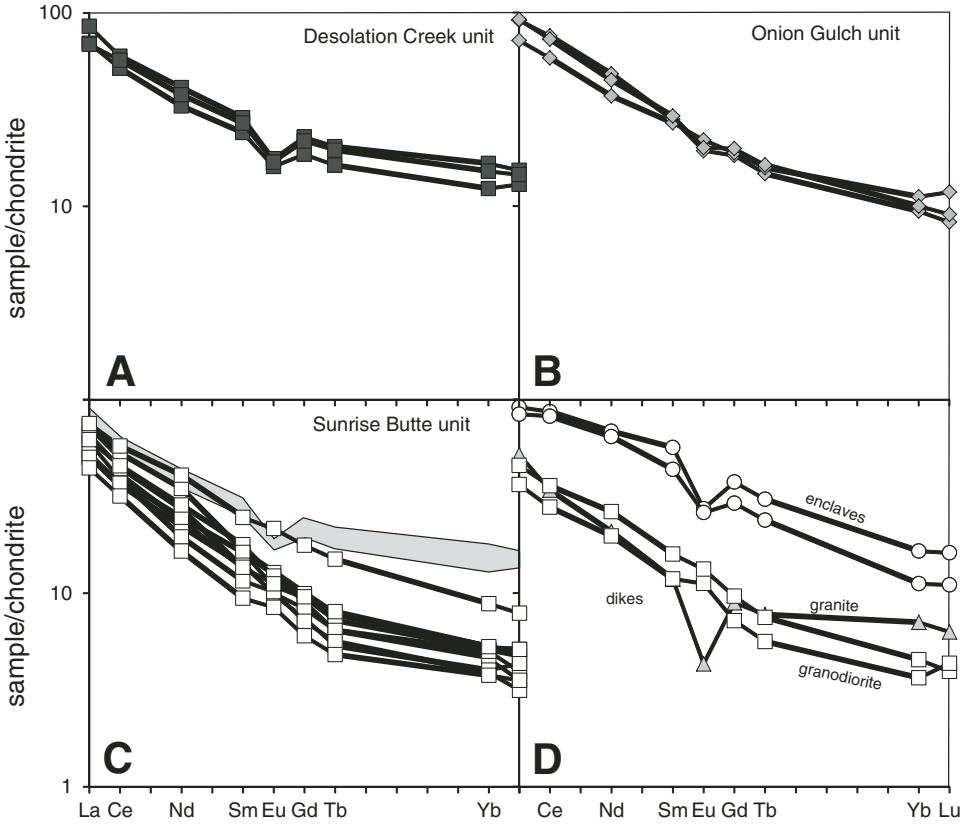

Figure 6. Chondrite-normalized (Sun and McDonough, 1989) rare earth element diagrams for rocks from the Sunrise Butte pluton. (A) Desolation Creek unit. (B) Onion Gulch unit. (C) Sunrise Butte unit. The shaded field is the outline of Desolation Creek rocks from A for comparison. (D) Magmatic enclaves and felsic dikes.

(gray square symbols) yielded an error-weighted average (2σ), initial ε_{Hf} value of 6.8 ± 1.6 (MSWD = 0.6). Initial ε_{Hf} values for the Onion Gulch and Sunrise Butte plutons (gray diamond and empty square symbols in Fig. 8, respectively) largely overlap with those from the Desolation Creek pluton, yielding values of 5.4 ± 1.5 (MSWD = 0.3) and 7.1 ± 1.5 (MSWD = 0.8), respectively. Initial ε_{Hf} values for all three plutons overlap values from other Late Jurassic to Early Cretaceous plutons in the Baker terrane (Schwartz et al., 2011b, 2014), although on average they extend to slightly lower values.

Compositional Variations Revealed by Magnetic Susceptibility

The bulk (volume) magnetic susceptibility is a measure of magnetization of a rock in the applied magnetic field and thus directly relates to the proportion, type, and composition of magnetic minerals (e.g., Hrouda and Kahan, 1991; Tarling and Hrouda, 1993). The bulk susceptibility has also proven to be a sensitive indicator of changes in chemical composition (e.g., Aydin et al., 2007) and redox state of granitoid magmas and has been used to define the oxidized magnetite and reduced ilmenite series of granitoid rocks (e.g., Ishihara, 1977, 2004).

In addition to geochemical data described already, we analyzed spatial variations in the bulk magnetic susceptibility in all units of the Sunrise Butte pluton (for a detailed magnetic fabric analysis, see Žák et al., 2012). The bulk susceptibility was measured on 271 specimens from 26 stations all over the pluton (Fig. 9A). The measurements were made using the MFK1-A Kappabridge in the Laboratory of Rock Magnetism at the Institute for Geology and Paleontology, Charles University in Prague.

On the map, the bulk susceptibilities define three distinct NW–SE-trending belts (Fig. 9A). The northeastern exposures of the Desolation Creek unit are characterized by the lowest susceptibilities on the order of 10^{-4} and can be thus regarded as paramagnetic (sensu Bouchez, 1997) or ilmenite-series rocks (Figs. 9A and 9B). In contrast, the northwestern exposures of the same unit and a narrow zone along the northeastern margin of the neighboring Sunrise Butte unit exhibit remarkably high susceptibilities on the order of 10^{-2} (Figs. 9A and 9B). Granitoids and dioritoids of this belt are thus ferromagnetic and can be attributed to the magnetite series. The contrasting paramagnetic and ferromagnetic mineralogies were also corroborated by measurements of susceptibility variations with temperature (supplemental information and Supplemental Figure DR1 [see footnote 1]). To the southwest, the susceptibilities are more variable, ranging from 10^{-4} to 10^{-2}, even within the same unit (Figs. 9A and 9B). Nevertheless, magnetite-series rocks are dominant.

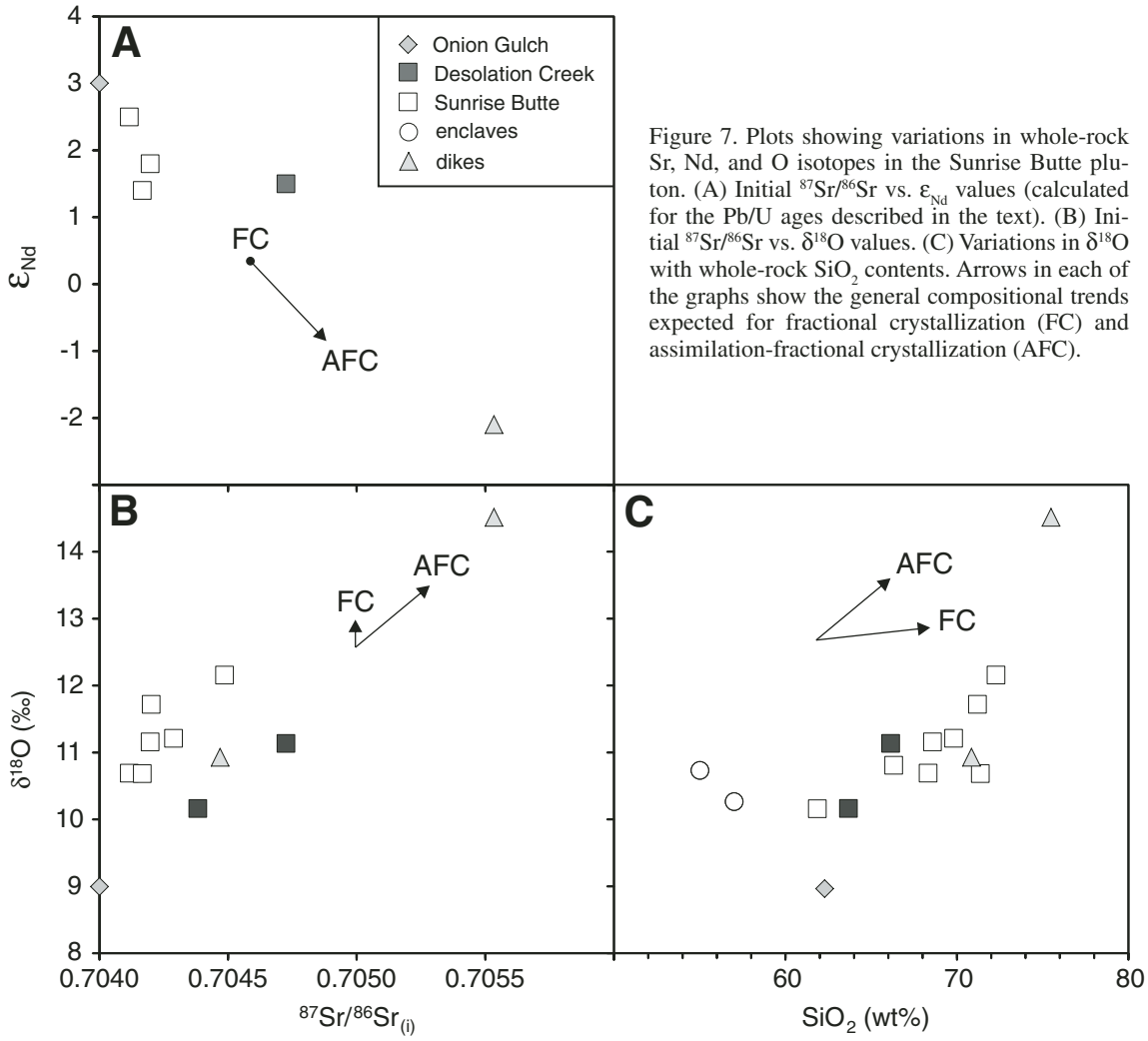

Figure 7. Plots showing variations in whole-rock Sr, Nd, and O isotopes in the Sunrise Butte pluton. (A) Initial $^{87}Sr/^{86}Sr$ vs. ε_{Nd} values (calculated for the Pb/U ages described in the text). (B) Initial $^{87}Sr/^{86}Sr$ vs. $\delta^{18}O$ values. (C) Variations in $\delta^{18}O$ with whole-rock SiO_2 contents. Arrows in each of the graphs show the general compositional trends expected for fractional crystallization (FC) and assimilation-fractional crystallization (AFC).

DISCUSSION

Origin and Evolution of the Magmas

The new $^{206}Pb/^{238}U$ ages presented here indicate that the Desolation Creek magma was emplaced during or shortly before arc-arc collision between the Wallowa and Olds Ferry arcs at 159–154 Ma (Schwartz et al., 2011a), and that emplacement of the Onion Gulch and Sunrise Butte magmas followed collision by several million years. Similar relationships have been documented in other areas of the Greenhorn subterrane (Johnson and Schwartz, 2009; Schwartz and Johnson, 2009; Schwartz et al., 2011b), as well as in the Bourne subterrane (Schwartz et al., 2014). In this section, we evaluate petrogenetic models pertaining to the origin of the Desolation Creek and Sunrise Butte magmas, as well as possible genetic relationships between the coeval Onion Gulch and Sunrise Butte units.

Major-element mass balance calculations (Bryan et al., 1969) were performed to test for fractional crystallization; in these calculations, a sum of the squares of the residuals (ssr) less than unity suggests a possible valid result. The parental and daughter compositions and the calculated fractionating mineral assemblage of each successful model were further tested using Sr and Y. Batch partial melting was tested using the REEs, Sr, and Y. The REEs, Sr, and Y were used because the ratios La/Yb and Sr/Y can be sensitive indicators of pressure (Moyen et al., 2010). The mineral-liquid partition coefficients from Schwartz et al. (2011b) were used in the trace-element calculations.

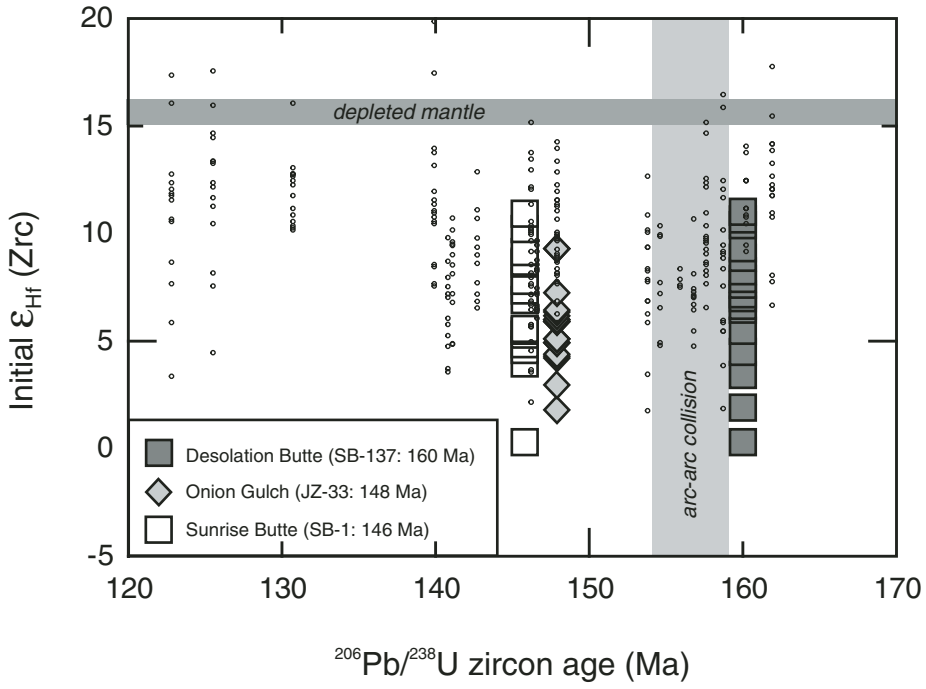

Figure 8. Zircon Lu-Hf isotopic data for rocks from the Sunrise Butte pluton. Initial Hf values were calculated at the time of crystallization using calculated weighted average $^{206}Pb/^{238}U$ ages (this study). Also shown in the graph are zircon Lu-Hf data for rocks from other plutons in the Blue Mountains Province (small circles; data from Schwartz et al., 2011b).

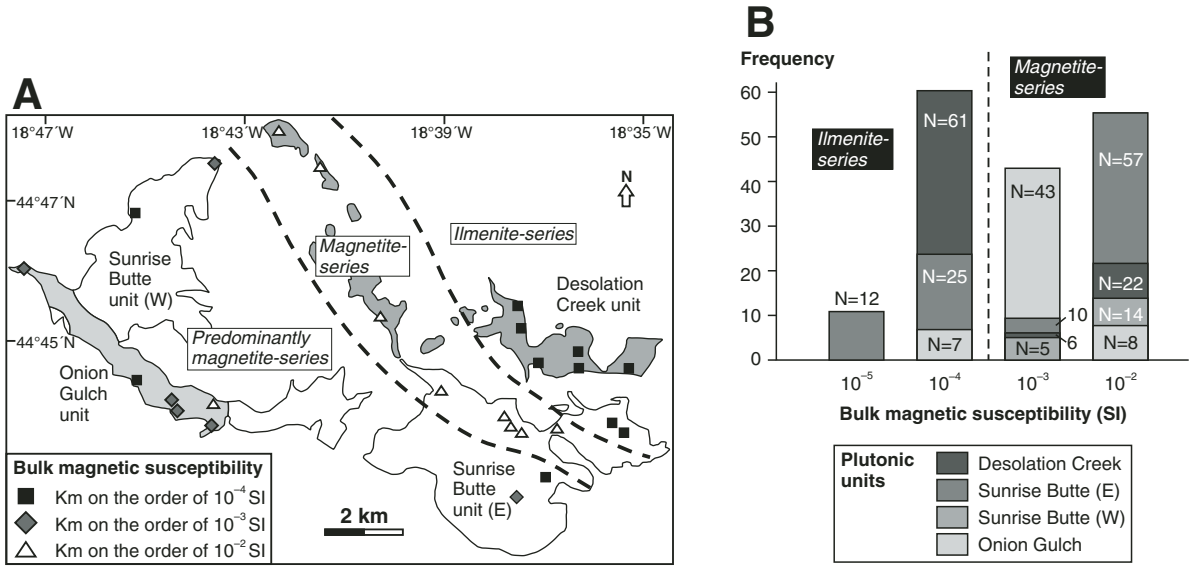

Figure 9. Results of magnetic susceptibility measurements. (A) Map of the bulk susceptibilities in the Sunrise Butte composite pluton (average values at each station). Susceptibility spatial variations define three distinct belts with the ilmenite-series granitoids to the northwest and magnetite-series granitoids to the southeast. (B) Histogram of the bulk susceptibilities of all analyzed specimens from the Sunrise Butte composite pluton. The histogram clearly shows a trend from the oldest ilmenite-series (Desolation Creek) to younger magnetite-series units.

Desolation Creek Unit

In comparison to most plutons in the Blue Mountains Province with similar SiO_2 contents, the Desolation Creek unit has the lowest Sr abundances (Fig. 5E). In addition, the Desolation Creek rocks exhibit moderate fractionation of the heavy (H) REEs from the light (L) REEs, along with negative Eu anomalies. These chemical signatures suggest an important role for plagioclase in the origin of the Desolation Creek magma. Such magmas can be produced by partial melting of metabasaltic rocks in the middle crust (in equilibrium with a plagioclase-rich but garnet-free residue), or by feldspar-dominated fractional crystallization of mantle-derived magma (± assimilation of crustal rocks).

Partial melting calculations were performed using a variety of metabasaltic source rock compositions from the Baker and Wallowa terranes. Chondrite-normalized REE patterns of calculated melts were compared to those of rocks from the Desolation Creek unit. The best matches were from those calculations using a flat to slightly LREE-enriched source rock pattern. All successful calculations are consistent with a garnet-absent and plagioclase-rich residual assemblage. For example, Figure 10A shows the results of one of these calculations, in which a pillow lava from Vinegar Hill was used as a potential source (see Schwartz et al., 2011a). The calculations predict a residual assemblage of hornblende (33%) + plagioclase (23%) + clinopyroxene (44%) for melt fractions between 0.1 and 0.3. However, this same residual assemblage will result in melts having much higher Sr/Y values than Desolation Creek rocks, which is not consistent with the data shown in Figure 10B. We conclude that the Desolation Creek magma was not the product of partial melting of known metabasaltic rocks in the Blue Mountains Province.

An alternative explanation for the origin of the Desolation Creek magma involves fractional crystallization of a similarly Sr-poor parental magma. A logical choice for such a parent composition is the Dixie Butte meta-andesite. The Dixie Butte meta-andesite complex, ~25 km to the south of the Desolation Creek unit (Fig. 1), consists of 610–670 m of flows of mostly basaltic andesite to andesite. Although the age of the meta-andesite complex has not been determined directly, it is considered to be Late Jurassic based on crosscutting relationships with, and lithologic similarities to, the Dixie Summit pluton (162.0 ± 2.9 Ma; Schwartz et al., 2011b). This age overlaps that of the Desolation Creek unit. Figure 5 shows whole-rock compositions from the Sunrise Butte pluton, along with whole-rock compositions for the Dixie Butte meta-andesite.

Desolation Creek compositions plot along an extension of the meta-andesite data trend (see especially Figs. 5C and 5E), so major- and trace-element calculations were performed to determine if the Desolation Creek magma could have been derived from magma similar in composition to the Dixie Butte meta-andesite. Major-element mass balance results suggest that the least siliceous Desolation Creek sample (sample SB-69A) could be derived from magma corresponding to the most siliceous Dixie Butte andesite (sample DBO19A; Schwartz et al., 2011b) by removal of a fractionating assemblage of plagioclase (An_{52}) + augite + orthopyroxene + Fe-Ti oxide + apatite (ssr = 0.765; model 1A in Table 3). Separation of this assemblage would lead to Y enrichment and a slight lowering

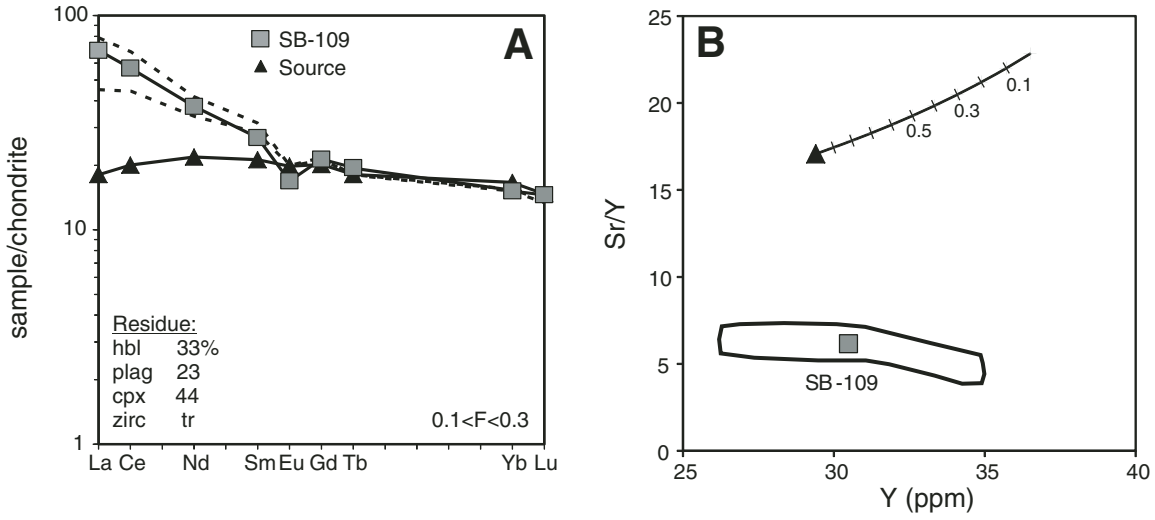

Figure 10. Results of partial melting calculations for the Desolation Creek unit. (A) Results using rare earth elements. Dashed lines represent calculated melt compositions for melt fractions (*F*) of 0.1 and 0.3. The source composition used is a pillow basalt from Vinegar Hill (within the Baker terrane; sample VH2–07–2B from Schwartz et al., 2011a). Abbreviations: hbl—hornblende; plag—plagioclase; cpx—clinopyroxene; zirc—zircon. (B) Plot of Sr/Y vs. Y, using the same residual assemblage as in A. Numbers beside the partial melting curve represent melt fractions. Outlined field represents all compositions from the Desolation Creek unit. Results using Sr and Y are inconsistent with those using the rare earth elements.

TABLE 3. RESULTS OF MAJOR-ELEMENT MASS BALANCE CALCULATIONS

Model	Parent	Plag	Cpx	Opx	Hbl	Gt	Mt	Sph	Apat	Daughter	Xan	F	ssr
1A	DB019A*	70.01	11.64	4.29			1.30		0.33	SB-69A	0.52	0.705	0.765
1B	SB-69A	45.02	6.38		45.23		2.71	0.52	0.14	SB-73	0.46	0.500	0.341
2A	VS3-1†		6.03		76.04	16.89		1.04		SB-94B		0.349	0.658

Notes: Abbreviations: Plag—plagioclase, Cpx—clinopyroxene, Opx—orthopyroxene, Hbl—hornblende, Gt—garnet, Mt—magnetite, Sph—sphene, Apat—apatite, Xan—mole fraction of the anorthite component in plagioclase, F—weight fraction of liquid, ssr—sum of the squares of the residuals. Mineral proportions are normalized to 100%.

*From Schwartz et al. (2011a).

†From Vallier (1995).

of the Sr/Y value in the residual liquid. In Figure 11, sample SB-69A plots near the calculated fractional crystallization curve at an *F* value between 0.6 and 0.7, which is consistent with the major-element mass balance results. Further fractional crystallization of an assemblage consisting of plagioclase (An_{46}) + augite + hornblende + Fe-Ti oxide + apatite + sphene would have led to SiO_2 enrichment in the residual liquid (sample SB-73; model 1B). Therefore, we conclude that the Desolation Creek magma most likely evolved by fractional crystallization from a mantle-derived magma similar in composition to the Dixie Butte meta-andesite.

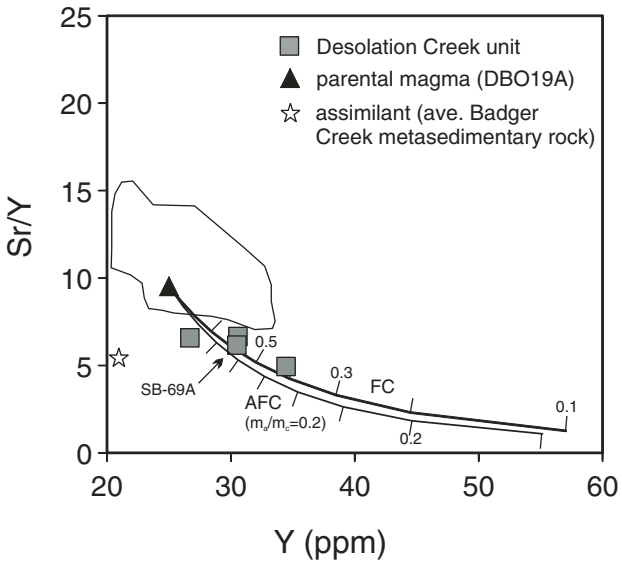

Figure 11. Results of fractional crystallization (FC) and assimilation-fractional crystallization (AFC; DePaolo, 1981) calculations for the Desolation Creek unit. Numbers beside the FC and AFC curves represent residual melt fractions. Outlined field represents compositions of Dixie Butte meta-andesite rocks. The parental magma composition used in the calculations is sample DBO19A (Schwartz et al., 2011b), and the assimilant used is an average of Badger Creek metasedimentary rock compositions (Schwartz et al., 2011a), which comprise the wall rocks at the level of exposure. Sample SB-109 plots near both FC and AFC curves for $F = 0.6–0.7$, consistent with results of mass balance calculations ($F = 0.704$; Table 3).

Sunrise Butte Unit

The presence of augite and orthopyroxene in rocks from the Onion Gulch unit suggests they crystallized from an evolved mantle-derived magma. The U-Pb zircon ages of the Onion Gulch unit overlap with those of the Sunrise Butte unit, indicating they were comagmatic. However, several factors argue against a cogenetic relationship between the two: (1) Onion Gulch and Sunrise Butte rocks have different mafic mineral assemblages, with the former dominated by augite and orthopyroxene and the latter consisting of hornblende and biotite; (2) Onion Gulch rocks exhibit an increase in K_2O (up to 2.26 wt%) with increasing SiO_2, whereas the more felsic rocks of the Sunrise Butte unit have lower K_2O contents (<1.9 wt%) that remain relatively constant with increasing SiO_2 (Fig. 5B); and (3) major-element mass balance calculations predict a range of plagioclase-rich fractionating assemblages (up to 26 wt% of the fractionating phases), which would lead to lower Sr abundances and more pronounced negative Eu anomalies in the derivative magma. The Sunrise Butte rocks do not exhibit these effects. Therefore, we conclude that the Sunrise Butte magma was not derived from the Onion Gulch magma by any crystal-liquid separation process.

The steeply fractionated REE patterns, high Sr, and low HREE and Y abundances in the Sunrise Butte rocks suggest that the magmas were in equilibrium with garnet, and that plagioclase was not a residual phase. In fact, samples from the Sunrise Butte unit have identical REE patterns and Sr/Y ratios to rocks from the Cornucopia Stock, magmas of which were emplaced into the Wallowa terrane (Fig. 1). Cornucopia magmas were generated by partial melting of low-K metabasaltic rocks comprising the deep crust of the Wallowa terrane, in equilibrium with a garnet + clinopyroxene + hornblende residue (Johnson et al., 1997). Given the underthrust nature of the Wallowa terrane (Schwartz et al., 2010), we tested the idea that the Sunrise Butte magma was generated by partial melting of deeply buried Wallowa terrane crust, similar to the style of Cornucopia magmatism.

We tested a variety of potential tholeiitic sources having slightly LREE-depleted to slightly LREE-enriched patterns (Balcer, 1980; Vallier, 1995; Kurz et al., 2012), which are characteristic of low-K metabasaltic rocks in the Wallowa terrane. Results using the REE abundances of several source compositions vary slightly but are generally consistent; they all predict a hornblende- and garnet-bearing, plagioclase-poor residual

assemblage and melt percentages between 10% and 40%. For example, Figure 12A shows the results of partial melting calculations using a source composition with a relatively flat REE pattern. In this diagram, chondrite-normalized REE patterns of the calculated melt compositions closely match those of the Sunrise Butte rocks for 20%–40% melting. Furthermore, the calculations predict a residual assemblage of hornblende + garnet + clinopyroxene.

Partial melting was also tested using Sr and Y abundances. In Figure 12B, using an average of the tholeiitic basalt compositions from Vallier (1995) as the source and the same residual assemblage as in Figure 12A, the calculated partial melting curve passes through the field of Sunrise Butte rock compositions for melt percentages of 5%–60%. However, it should be noted that the Sunrise Butte sample used in Figure 12A (sample SB-94B) plots along the partial melting curve at a melt fraction of ~0.2, which is consistent with results using the REEs. These results demonstrate that the high La/Yb and Sr/Y characteristics of the Sunrise Butte unit arose from partial melting of a metabasaltic source at a depth greater than that required for the stability of garnet.

Major-element mass balance calculations were also performed (Table 3), using hornblende and garnet compositions from Matsell et al. (2012). Results of these calculations suggest that the Sunrise Butte magma could be derived from a mafic protolith in equilibrium with a hornblende + garnet + clinopyroxene residue. Although the major-element calculations predict residual phase proportions and melt fractions (*F*) different to those predicted using trace elements (Fig. 12), they are consistent with a residual assemblage having hornblende >> garnet.

Tectonic Implications

The Sunrise Butte pluton is composed of three distinct intrusions: (1) an older (ca. 160 Ma) body of hornblende biotite quartz diorite/tonalite (the Desolation Creek unit), (2) a younger (ca. 148 Ma) unit of two-pyroxene diorite (the Onion Gulch unit), and (3) an intrusion of hornblende biotite tonalite/granodiorite (the Sunrise Butte unit) that is coeval with the Onion Gulch unit. These units are geochemically distinct, which suggests different sources and petrogenetic histories. This notion is further supported by magnetic susceptibilities measured in the pluton (Fig. 9A), in which rocks from the Desolation Creek unit are paramagnetic, belonging to the ilmenite series, and those from the Sunrise Butte unit are predominantly ferromagnetic (belonging to the magnetite series). Red biotite in rocks from the Desolation Creek unit is higher in total Al than biotite from the Sunrise Butte unit, and this is thus also suggestive of reducing conditions in the magma (Lalonde and Bernard, 1993). The magnetic characteristics of the magmas could have been inherited from their sources, recording a transition from a reduced, mantle-derived source to a deep crustal, more-oxidized source with time (e.g., Ishihara, 2004). The paramagnetic signature of the Desolation Creek unit could also have been further enhanced through in situ assimilation of the surrounding serpentinitic wall rocks and/or graphite-bearing metasedimentary rocks of the Badger Creek unit (e.g., Ague and Brimhall, 1988; Malvoisin et al., 2012; Tomkins et al., 2012). In situ assimilation is consistent with the positive correlations in whole-rock $\delta^{18}O$ values and SiO_2 contents, and the negative correlation in ε_{Nd}, with initial $^{87}Sr/^{86}Sr$ values (Fig. 7).

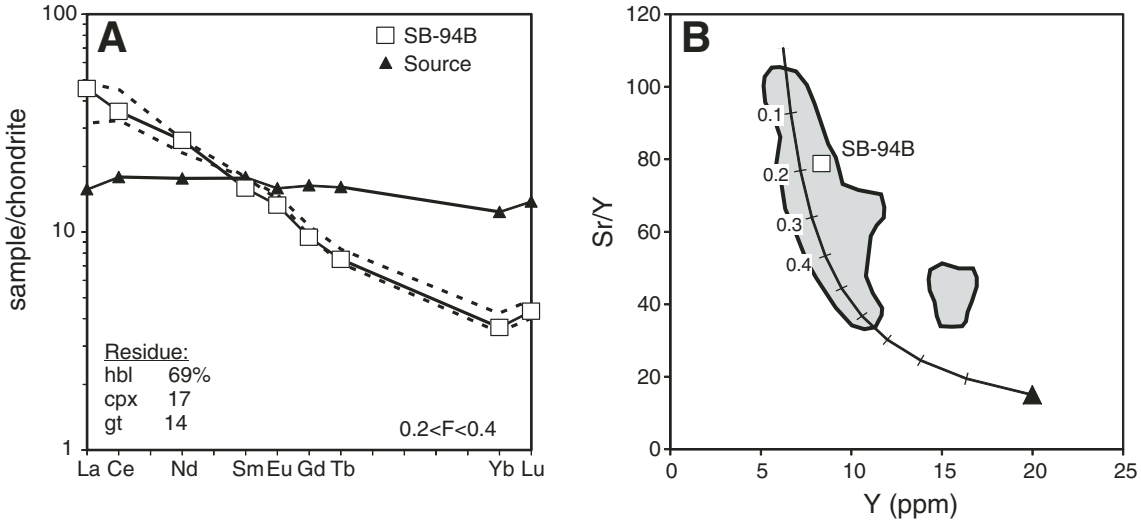

Figure 12. Results of partial melting calculations for the Sunrise Butte unit. (A) Results using rare earth elements. Dashed lines represent calculated melt compositions for melt fractions (*F*) of 0.2 and 0.4. The source composition used in the calculations is sample Hcm-16 from Balcer (1980). Abbreviations: hbl—hornblende; gt—garnet; cpx—clinopyroxene. (B) Plot of Sr/Y vs. Y, using the same residual assemblage as in A. Numbers beside the partial melting curve represent melt fractions. Shaded fields represent all compositions from the Sunrise Butte unit. Note that sample SB-94B plots near the partial melting curve at an *F* value of ~0.2, consistent with the results in A.

The Sunrise Butte composite pluton preserves a record of magmatism in response to arc-arc collision and resultant crustal thickening (Fig. 13). Subduction-related magmatism (the Desolation Creek unit) occurred as the Wallowa island arc neared the Olds Ferry island arc (top panel in Fig. 13). The ensuing collision (ca. 159–154 Ma; Schwartz et al., 2011a) resulted in thrusting of the Baker accretionary wedge/forearc terrane over the Wallowa and Olds Ferry arcs (middle panel in Fig. 13). Partial melting of the thickened arc crust resulted in the generation of high-Sr/Y magma (the Sunrise Butte unit) that was emplaced into relatively shallow levels of the Baker terrane crust (the Greenhorn subterrane); the heat necessary for partial melting was provided by mantle-derived magma (the Onion Gulch unit) from the now-waning subduction system (bottom panel in Fig. 13).

Similar relationships among low-Sr/Y magmatism, crustal thickening, and generation of high-Sr/Y magmas have been

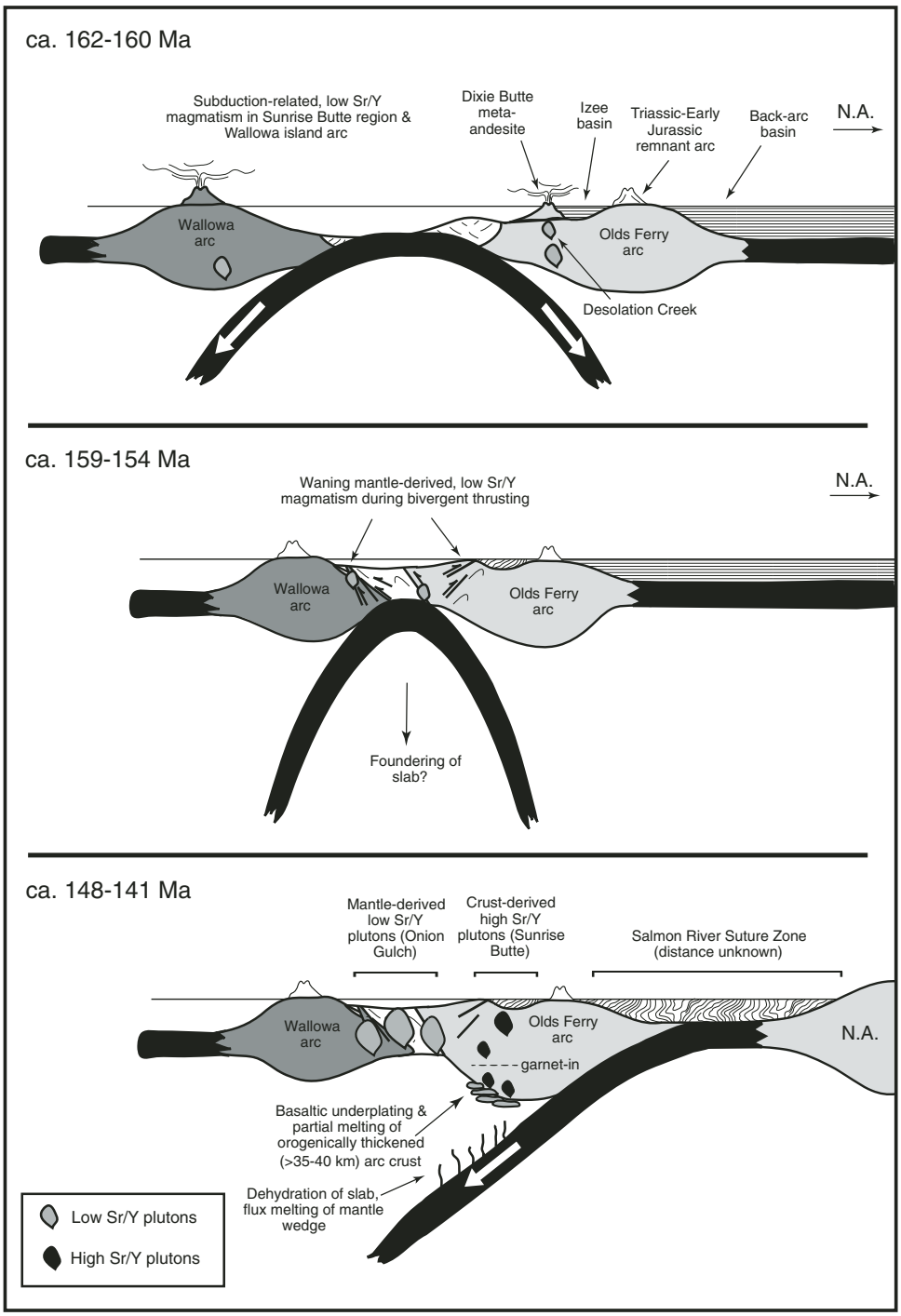

Figure 13. Tectonic model for the generation of low- and high-Sr/Y plutons in the central portion of the Blue Mountains Province, modified from Schwartz et al. (2011b). N.A.—North America.

observed elsewhere in the central Blue Mountains Province. South of the Sunrise Butte pluton, small intrusions in the Dixie Butte area show similar composition-age relationships (Schwartz et al., 2011b). There, pre- and syncollisional subduction-related magmatism resulted in low-Sr/Y intrusions (ca. 162–158 Ma) and the Dixie Butte meta-andesite flows (ca. 162 Ma; Schwartz et al., 2011b). Arc-arc collision was accompanied by a magmatic lull, but it was followed shortly after by the emplacement of several high- and low-Sr/Y intrusions (ca. 148–145 Ma; Schwartz et al., 2011b). Schwartz et al. (2011b) suggested that Late Jurassic shortening led to ≥12 km of crustal thickening in this area.

In the Bald Mountain batholith (Fig. 1), ~50 km northeast of the Sunrise Butte pluton, noritic and granitic magmas of low-Sr/Y affinity (ca. 157–155 Ma) were emplaced, followed by high-Sr/Y tonalitic magmas (ca. 147–141 Ma) that comprise the bulk of the exposed area of the batholith (Schwartz et al., 2014). Here again, the same sequence of subduction-related magmatism, arc-arc collision, crustal thickening, and generation of high-Sr/Y magmas from tectonically thickened crust is observed.

Geochemical models for the generation of high-Sr/Y magmas from metabasaltic rocks at all three of these localities point to garnet-bearing, hornblende-rich (but plagioclase-absent) residual assemblages. Such residual assemblages are produced at high pressures (>10 kbar or >35 km depth) by dehydration melting reactions of the form:

$$\text{hornblende} + \text{plagioclase} \rightarrow \text{clinopyroxene} + \text{garnet} + \text{hydrous melt},$$

in which plagioclase is the limiting reactant (Winther and Newton, 1991; Wolf and Wyllie, 1993). An abundance of residual hornblende and the absence of plagioclase are suggestive of melting under water-rich conditions (Weinberg and Hasalová, 2015); additional water could have come from exsolution of mantle-derived magmas (which would have also contributed to the heat budget necessary for partial melting) or the breakdown of hydrous phases other than amphibole. Preliminary results from a study of tonalitic and trondhjemitic veins in migmatized amphibolites along the Salmon River suture zone suggest that the water needed to stabilize hornblende and destabilize plagioclase may have come from the breakdown of epidote during prograde metamorphism (Richter et al., 2012; Richter and Johnson, 2014). As pointed out by Johnson et al. (1997), blocks of garnet hornblendite (with up to 80% hornblende) in serpentinite-matrix mélange were exhumed along the Connor Creek fault ~50 km southeast of the Dixie Butte area (Matsell et al., 2012). Although these rocks may not represent the solid residue of a partial melting event, they do illustrate that such hornblende-rich garnet-bearing (and plagioclase-absent) metamorphic rocks occur in the Blue Mountains Province.

Results of this research are consistent with the relationships among arc-arc or arc-continent collisions, crustal thickening, and the generation of high-Sr/Y magmas observed in other segments of the North American Cordillera (Gromet and Silver, 1987; Barnes et al., 1996, 2006; Tulloch and Kimbrough, 2003; Girardi et al., 2012). For example, deformation and crustal thickening associated with the Nevadan orogeny in the Klamath Mountains (ca. 153–150 Ma; Harper et al., 1994) marked the transition from low-Sr/Y magmatism to a later stage of predominantly high-Sr/Y magmatism (Barnes et al., 1996, 2006). We suggest that crustal shortening in the Klamath Mountains and Blue Mountains Provinces was related to the same event, and we envision the Late Jurassic collapse of an extensional basin represented by the Josephine ophiolite in the Klamaths, the coeval Ingalls ophiolite in the central Cascades (MacDonald et al., 2008), and the Baker terrane in the Blue Mountains. Crustal shortening in the Blue Mountains Province (ca. 159–154 Ma; Schwartz et al., 2011a) predates that in the Klamath Mountains (ca. 153–150 Ma), which suggests that the closure of the basin progressed from north to south.

CONCLUSIONS

The Late Jurassic–Early Cretaceous Sunrise Butte pluton, in the central region of the Blue Mountains Province, records distinct stages related to the collision of two volcanic arcs. An early stage of mantle-derived magmatism, characterized by the Desolation Creek unit, occurred as subduction consumed the intervening oceanic crust between the Wallowa and Olds Ferry arcs. A period of magmatic quiescence followed as the crust thickened in response to underthrusting of the Wallowa arc beneath the accretionary wedge (the Bourne subterrane). Magmatism recommenced with partial melting at the base of the overthickened crust, resulting in the generation and emplacement of high-Sr/Y magma (the Sunrise Butte unit).

Temporal similarities in crustal shortening, deformation, and magmatism observed in the Blue Mountains and the Klamath Mountains Provinces (and possibly the Ingalls ophiolite complex) suggest they are linked to the same regional event. Studies that potentially connect tectonic events in the Blue Mountains Province to those in the Klamath Mountains provide a crucial first step in developing a comprehensive understanding of the North American Cordillera.

ACKNOWLEDGMENTS

This study stems from work done toward an M.S. degree at Texas Tech University by Walton, and most of the field work and whole-rock elemental analyses were performed by him. Thoughtful reviews by Edward Lidiak and John Shervais greatly improved the manuscript. We thank Rob Holler and Joseph Gravlee at the University of Alabama for obtaining mineral analyses and Ryan Jeffcoat for assistance in the field. Discussions with Mark Ferns greatly improved our understanding of Blue Mountains geology. Melanie Barnes helped with inductively coupled plasma–atomic emission spectrometry analyses, and James Browning provided assistance with oxygen isotope analyses. This project was funded in part by National Science Foundation grants EAR-0911735 (to Johnson), EAR-0911681

(to Schwartz), and EAR-9117103 (to Barnes), by a grant from the Organized Research Committee at the University of Houston–Downtown (to Johnson), and by the Grant Agency of the Czech Republic through grant no. P210/12/1385 (to Žák).

APPENDIX. ANALYTICAL METHODS

Major- and Trace-Element Analyses

Sample powders were prepared in an alumina ceramic shatterbox, fused with a $LiBO_2$ flux, and dissolved in a weak HCl solution. Sample solutions were analyzed for major-element oxides, Sc, V, Cr, Ni, Cu, Zn, Nb, Sr, Ba, Y, and Zr by inductively coupled plasma–atomic emission spectrometry (ICP-AES) at Texas Tech University and the University of Houston–Downtown. Rubidium was analyzed by flame emission spectrometry. Selected samples were analyzed for the REEs, Co, Sb, Cs, Hf, Ta, and Th by instrumental neutron activation at Oregon State University.

Mineral Chemistry

Mineral compositions were determined using a JEOL JXA-8600 Superprobe at the University of Alabama. Electron probe operating conditions were 15 kV accelerating potential, 10–20 nA beam current (depending on the mineral being analyzed), and 1 µm beam diameter. On-line corrections were made with a ZAF procedure, and a suite of natural minerals was used as standards.

Isotope Analyses

Strontium isotope compositions were determined at the U.S. Geological Survey (Menlo Park, California), and neodymium isotope compositions were determined at Rice University (Houston, Texas) using methods described in Barnes et al. (2001).

Oxygen was liberated from whole-rock powders by reaction with BrF_5 (Clayton and Mayeda, 1963). Oxygen was converted to CO_2 by reacting with hot graphite, and CO_2 yields were measured online. Samples with CO_2 yields of $100\ ^{-0.5}/_{+1.0\%}$ were considered acceptable. Oxygen isotope ratios were determined on a VG SIRA-12 dual-inlet gas source mass spectrometer at Texas Tech University and are reported relative to Vienna standard mean ocean water (VSMOW). The cumulative value for NBS-28 during the course of this study was 9.49‰ ± 0.2‰.

U-Pb Geochronology

Sample Preparation

Zircons were separated from whole-rock samples following standard crushing methods involving density (Gemini table and heavy liquids) and magnetic (Frantz isodynamic separator) separation techniques. Nonmagnetic zircons (at 1.5 amps) were handpicked at the University of Alabama to obtain optically clear, colorless grains free or largely free of mineral and fluid inclusions. Zircons were mounted in epoxy and imaged on a Gatan MiniCL detector attached to the JEOL 8600 at the University of Alabama.

SHRIMP-RG U-Pb Zircon Geochronology

Methods for SHRIMP-RG analyses closely follow those outlined by Compston et al. (1984) and Williams (1998). Samples were analyzed in continuous analytical sessions with standards run for every 3–4 unknowns. A gem-quality zircon, CZ3, with 550 ppm U was used for U concentration determinations, and grains of R33, a 419 Ma quartz diorite from the Braintree complex, Vermont, were used as the Pb/U age standard (John Aleinikoff, 2001, personal commun.). Raw data were reduced using SQUID (Ludwig, 2001), and all ages were calculated with Isoplot 3.00 (Ludwig, 2003). Corrections for common Pb in zircon were made following methods of Tera and Wasserburg (1972) using measured $^{207}Pb/^{206}Pb$ and $^{238}U/^{206}Pb$ ratios and an age-appropriate Pb isotopic composition from Stacey and Kramers (1975). Pb/U ages are reported in Table 1 and given at the 2σ level, unless otherwise noted.

Lu-Hf Isotope Analyses

Hf isotope data were collected using a New Wave 193 nm ArF laser-ablation system coupled to a Nu Plasma high-resolution (HR) inductively coupled plasma–mass spectrometer (ICP-MS) at the University of Arizona. Ablation was performed in a New Wave SuperCell™, and sample aerosol was transported with He carrier gas through Teflon-lined tubing, where it was mixed with Ar gas before introduction to the plasma torch. The multicollector (MC) ICP-MS utilizes 12 Faraday detectors equipped with 3×10^{11} Ω resistors and four discrete dynode ion counters, which remain fixed as beams are directed into them via an electrostatic zoom lens. For Hf analyses, masses 171, 173, 175, 176, 177, 178, 179, and 180 were all measured simultaneously in Faraday collectors. Pure Hf solutions and Hf solutions doped with various amounts of Yb and Lu were introduced in Ar carrier gas via a Nu DSN-100 desolvating nebulizer.

Accurate in situ measurement of Hf isotopes in zircon is made difficult by the isobaric interferences of ^{176}Yb and ^{176}Lu on ^{176}Hf, the correction of which has been discussed in detail in previous publications (e.g., Griffin et al., 2002; Woodhead et al., 2004; Iizuka and Hirata, 2005; Hawkesworth and Kemp, 2006; Gerdes and Zeh, 2009; Wu et al., 2006; Kemp et al., 2009). Properly correcting for ^{176}Yb (and to a lesser degree ^{176}Lu) is critical given that $^{176}Yb/^{176}Hf$ of typical zircons is commonly between 10% and 30% and can be as much as 70%. $^{179}Hf/^{177}Hf$ was used for mass bias corrections, and an exponential mass bias function was used in all calculations. The values of ^{173}Yb and ^{171}Yb, which are interference free, were monitored during the Hf analysis in order to calculate Yb mass bias (β_{Yb}) and the contribution of Yb to the measurement of $^{176}(Hf + Lu + Yb)$. Because the magnitude of the Yb correction is large, small inaccuracies in the Yb mass bias can lead to large analytical errors (Woodhead et al., 2004). Unlike $^{179}Hf/^{177}Hf$, the precision of the $^{173}Yb/^{171}Yb$ measurement, and consequently the accuracy of β_{Yb}, is dependent upon the Yb signal intensity. At ^{171}Yb intensities of less than 0.015 V, it becomes very difficult to reliably estimate β_{Yb}, and for those analyses, Hf mass bias (β_{Hf}) was used to correct $^{176}Yb/^{171}Yb$. Chu et al. (2002) and Woodhead et al. (2004) have shown that Hf and Yb exhibit slightly different fractionation behavior, which we also observed. Although it is therefore not ideal to use Hf fractionation factors to correct for Yb mass bias, low-Yb zircons require relatively minor correction, and as such it is possible to use β_{Hf} without introducing large errors to the corrected $^{176}Hf/^{177}Hf$. The Lu correction was done by monitoring ^{175}Lu and using $^{176}Lu/^{175}Lu = 0.02653$ (Patchett, 1983) and β_{Yb}, assuming that Lu behaves similarly to Yb. All corrections were performed on a line-by-line basis, and in all cases, Hf and Yb isotope data were normalized to $^{179}Hf/^{177}Hf = 0.72350$ (Patchett and Tatsumoto, 1980) and $^{173}Yb/^{171}Yb = 1.132338$ (Vervoort et al., 2004), respectively. A ^{176}Lu decay constant of 1.876×10^{-11} (Scherer et al., 2001) was used in all calculations. Chondritic values of Bouvier et al. (2008) were adopted for the calculation of ε_{Hf} values.

Analyses of pure Hf solutions, as well as Hf solutions doped with variable amounts of Yb and Lu, were performed in order to test our ability to reliably correct for Yb and Lu interferences. Solution analyses were run in three blocks of 20 measurements, with additional background measurements being automatically performed between blocks. Backgrounds were measured using an electrostatic analyzer deflection

for 60 s at the start of the run, and measurements were integrated over 5 s. For 10 ppb solutions, total Hf beams of about 5 V were achieved (this is the maximum possible with our 3×10^{11} Ω resistors). Solution data were collected during many analytical sessions over the course of this study, and Hf standard solution measurements were always made after instrument tuning and before acquisition of laser data. Repeated analysis of JMC 475 (n = 71) in the Arizona LaserChron laboratory yielded a weighted mean of $^{176}Hf/^{177}Hf$ = 0.282159 ± 15, which is nearly identical to the accepted JMC 475 value of 0.282160 (Vervoort et al., 2004). No normalization of the data to JMC 475 was performed. Hf Spex solution, although not an ultrapure interlaboratory standard, was also analyzed and found to be isotopically the same as JMC 475 (Hf Spex $^{176}Hf/^{177}Hf$ = 0.282159 ± 12). Hf Spex solutions doped with natural Yb and Lu produced corrected $^{176}Hf/^{177}Hf$ values similar to that of the pure solution, although scatter in the high (Yb + Lu)/Hf data was greater. No statistical correlation was found between $^{176}Hf/^{177}Hf$ and $^{176}(Lu + Yb)/^{176}Hf$, indicating that Yb and Lu interferences were adequately removed.

Laser ablation was done using a 40-µm-diameter spot and a hit rate of 7 Hz. The laser was run in constant energy mode with output energy of 8 mJ/pulse, which corresponds to an energy density of about 2 J/cm^2 and an estimated drill rate of 0.7 µm/s. The in situ analytical routine began with a 40 s on-peak background measurement followed by 60 s of laser ablation with a 1 s data integration time. This resulted in a laser pit that was ~50 µm in depth and 35 µm in diameter. All corrections were automatically calculated during the run on a line-by-line basis, and a 2σ filter was applied to each 60 measurement data block offline to remove outliers.

REFERENCES CITED

Ague, J.J., and Brimhall, G.H., 1988, Magmatic arc asymmetry and distribution of anomalous plutonic belts in the batholiths of California: Effects of assimilation, crustal thickness, and depth of crystallization: Geological Society of America Bulletin, v. 100, p. 912–927, doi:10.1130/0016-7606(1988)100<0912:MAAADO>2.3.CO;2.

Anderson, J.L., and Smith, D.R., 1995, The effects of temperature and fO_2 on the Al-in-hornblende barometer: American Mineralogist, v. 80, p. 549–559.

Armstrong, R.L., Taubeneck, W.H., and Hales, P.O., 1977, Rb–Sr and K–Ar geochronometry of Mesozoic granitic rocks and their Sr isotopic composition, Oregon, Washington, and Idaho: Geological Society of America Bulletin, v. 88, p. 397–411, doi:10.1130/0016-7606(1977)88<397:RAKGOM>2.0.CO;2.

Avé Lallemant, H.G., 1995, Pre-Cretaceous tectonic evolution of the Blue Mountains province, northeastern Oregon: U.S. Geological Survey Professional Paper 1438, p. 271–304.

Aydin, A., Ferré, E.C., and Aslan, Z., 2007, The magnetic susceptibility of granitic rocks as a proxy for geochemical composition: Example from the Saruhan granitoids, NE Turkey: Tectonophysics, v. 441, p. 85–95, doi:10.1016/j.tecto.2007.04.009.

Barker, F., 1979, Trondhjemite: Definition, environment, and hypotheses of origin, *in* Barker, F., ed., Trondhjemites, Dacites, and Related Rocks: New York, Elsevier, p. 1–12.

Balcer, D.E., 1980, $^{40}Ar/^{39}Ar$ Ages and REE Geochemistry of Basement Terranes in the Snake River Canyon, Northeastern Oregon–Western Idaho [M.S. thesis]: Columbus, Ohio, Ohio State University, 111 p.

Barnes, C.G., Petersen, S.W., Kistler, R.W., Prestvik, T., and Sundvoll, B., 1992, Tectonic implications of isotopic variation among Jurassic and Early Cretaceous plutons, Klamath Mountains: Geological Society of America Bulletin, v. 104, p. 117–126, doi:10.1130/0016-7606(1992)104<0117:TIOIVA>2.3.CO;2.

Barnes, C.G., Petersen, S.W., Kistler, R.W., Murray, R., and Kays, M.A., 1996, Source and tectonic implications of tonalite–trondhjemite magmatism in the Klamath Mountains: Contributions to Mineralogy and Petrology, v. 123, p. 40–60, doi:10.1007/s004100050142.

Barnes, C.G., Burton, B.R., Burling, T.C., Wright, J.E., and Karlsson, H.R., 2001, Petrology and geochemistry of the late Eocene Harrison Pass pluton, Ruby Mountains core complex, northeastern Nevada: Journal of Petrology, v. 42, p. 901–929, doi:10.1093/petrology/42.5.901.

Barnes, C.G., Snoke, A.W., Harper, G.D., Frost, C.D., McFadden, R.R., Bushey, J.C., and Barnes, M.A.W., 2006, Arc plutonism following regional thrusting: Petrology and geochemistry of syn- and post-Nevadan plutons in the Siskiyou Mountains, Klamath Mountains province, California, *in* Snoke, A.W., and Barnes, C.G., eds., Geological Studies in the Klamath Mountains Province, California and Oregon: A Volume in Honor of William P. Irwin: Geological Society of America Special Paper 410, p. 357–376, doi:10.1130/2006.2410(17).

Bouchez, J.L., 1997, Granite is never isotropic: An introduction to AMS studies of granitic rocks, *in* Bouchez, J.L., Hutton, D.H.W., and Stephens, W.E., eds., Granite: From Segregation of Melt to Emplacement Fabrics: Dordrecht, Kluwer Academic Publishers, p. 95–112.

Bouvier, A., Vervoort, J.D., and Patchett, P.J., 2008, The Lu-Hf and Sm-Nd isotopic composition of CHUR: Constraints from unequilibrated chondrites and implications for the bulk composition of terrestrial planets: Earth and Planetary Science Letters, v. 273, p. 48–57, doi:10.1016/j.epsl.2008.06.010.

Brandon, A.D., and Smith, A.D., 1994, Mesozoic granitoid magmatism in southeast British Columbia: Implications for the origin of granitoid belts in the North American Cordillera: Journal of Geophysical Research, v. 99, p. 11879–11896, doi:10.1029/94JB00336.

Brooks, H.C., Ferns, M.L., Wheeler, G.R., and Avery, D.G., 1983, Geology and Gold Deposits Map of the Northeast Quarter of the Bates Quadrangle, Baker and Grant Counties, Oregon: Oregon Department of Geology and Mineral Industries Map GMS-29, scale 1:24,000.

Bryan, W.B., Finger, L.W., and Chayes, F., 1969, Estimating proportions in petrographic mixing equations by least squares approximation: Science, v. 163, p. 926–927, doi:10.1126/science.163.3870.926.

Chu, N.C., Taylor, R.N., Chavagnac, V., Nesbitt, R.W., Boella, R.M., Milton, J.A., German, C.R., Bayon, G., and Burton, K., 2002, Hf isotope ratio analysis using multi-collector inductively coupled plasma mass spectrometry: An evaluation of isobaric interference corrections: Journal of Analytical Atomic Spectrometry, v. 17, p. 1567–1574, doi:10.1039/b206707b.

Clayton, R.N., and Mayeda, T., 1963, The use of bromine pentafluoride in the extraction of oxygen from oxides and silicates for isotopic analysis: Geochimica et Cosmochimica Acta, v. 27, p. 43–52, doi:10.1016/0016-7037(63)90071-1.

Compston, W., Williams, I.S., and Meyer, C., 1984, U-Pb geochronology of zircons from lunar breccia 73217 using a sensitive high mass-resolution ion microprobe: Journal of Geophysical Research, v. 89, supplement 2, p. B525–B534, doi:10.1029/JB089iS02p0B525.

DeCelles, P.G., Ducea, M.N., Kapp, P., and Zandt, G., 2009, Cyclicity in Cordilleran orogenic systems: Nature Geoscience, v. 2, p. 251–257, doi:10.1038/NGEO469.

DePaolo, D.J., 1981, Trace element and isotopic effects of combined wallrock assimilation and fractional crystallization: Earth and Planetary Science Letters, v. 53, p. 189–202, doi:10.1016/0012-821X(81)90153-9.

Dorsey, R.J., and LaMaskin, T.A., 2007, Stratigraphic record of Triassic–Jurassic collisional tectonics in the Blue Mountains Province, northeastern Oregon: American Journal of Science, v. 307, p. 1167–1193, doi:10.2475/10.2007.03.

Drummond, M.S., and Defant, M.J., 1990, A model for trondhjemite–tonalite–dacite genesis and crustal growth via slab melting: Archean to modern comparisons: Journal of Geophysical Research, v. 95, p. 21503–21521, doi:10.1029/JB095iB13P21503.

Ducea, M.N., 2001, The California Arc; thick granitic batholiths, eclogitic residues, lithospheric-scale thrusting, and magmatic flare-ups: GSA Today, v. 11, no. 11, p. 4–10.

Evans, J.G., 1989, Geologic Map of the Desolation Butte Quadrangle, Grant and Umatilla Counties, Oregon: U.S. Geological Survey Map GQ-1654, scale 1:62,500.

Ferns, M.L., and Brooks, H.C., 1995, The Bourne and Greenhorn subterranes of the Baker terrane, northeastern Oregon: Implications for the evolution of the Blue Mountains island arc system, *in* Vallier, T.L., and Brooks, H.C., eds., Geology of the Blue Mountains Region of Oregon, Idaho, and Washington: Petrology and Tectonic Evolution of Pre-Tertiary Rocks of the Blue Mountains Region: U.S. Geological Survey Professional Paper 1438, p. 331–358.

Ferns, M.L., Brooks, H.C., and Wheeler, G.R., 1984, Geology and Gold Deposits Map of the Northwest Quarter of the Bates Quadrangle, Grant County, Oregon: Oregon Department of Geology and Mineral Industries Map GMS-31, scale 1:24,000.

Fleck, R.J., and Criss, R.E., 2007, Location, age, and tectonic significance of the Western Idaho Suture Zone, *in* Kuntz, M.A., and Snee, L.W., eds., 2007, Geological Studies of the Salmon River Suture Zone and Adjoining Areas, West-Central Idaho and Eastern Oregon: U.S. Geological Survey Professional Paper 1738, 202 p.

Frost, B.R., Barnes, C.G., Collins, W.J., Arculus, R.J., Ellis, D.J., and Frost, C.D., 2001, A geochemical classification for granitic rocks: Journal of Petrology, v. 42, p. 2033–2048, doi:10.1093/petrology/42.11.2033.

Gerdes, A., and Zeh, A., 2009, Zircon formation versus zircon alteration—New insights from combined U-Pb and Lu-Hf in-situ LA-ICP-MS analyses, and consequences for the interpretation of Archean zircon from the Central Zone of the Limpopo belt: Chemical Geology, v. 261, p. 230–243, doi:10.1016/j.chemgeo.2008.03.005.

Getty, S.R., Selverstone, J., Wernicke, B.P., Jacobsen, S.B., Aliberti, E., and Lux, D.R., 1993, Sm-Nd dating of multiple garnet growth events in an arc-continent collision zone, northwestern U.S. Cordillera: Contributions to Mineralogy and Petrology, v. 115, p. 45–57, doi:10.1007/BF00712977.

Giorgis, S., McClelland, W., Fayon, A., Singer, B.S., and Tikoff, B., 2008, Timing of deformation and exhumation in the western Idaho shear zone, McCall, Idaho: Geological Society of America Bulletin, v. 120, p. 1119–1133, doi:10.1130/B26291.1.

Girardi, J.D., Patchett, P.J., Ducea, M.N., Gehrels, G.E., Cecil, M.R., Rusmore, M.E., Woodsworth, G.J., Pearson, D.M., Manthei, C., and Wetmore, P., 2012, Elemental and isotopic evidence for granitoid genesis from deep-seated sources in the Coast Mountains batholith, British Columbia: Journal of Petrology, v. 53, p. 1505–1536, doi:10.1093/petrology/egs024.

Griffin, W.L., Wang, X., Jackson, S.E., Pearson, N.J., O'Reilly, S.Y., Xu, X., and Zhou, X., 2002, Zircon chemistry and magma mixing, SE China: In situ analysis of Hf isotopes, Tonglu and Pingtan igneous complexes: Lithos, v. 61, p. 237–269, doi:10.1016/S0024-4937(02)00082-8.

Gromet, L.P., and Silver, L.T., 1987, REE variations across the Peninsular Ranges batholith: Implications for batholithic petrogenesis and crustal growth in magmatic arcs: Journal of Petrology, v. 28, p. 75–125, doi:10.1093/petrology/28.1.75.

Harper, G.D., Saleeby, J.B., and Heizler, M., 1994, Formation and emplacement of the Josephine ophiolite and the Nevadan orogeny in the Klamath Mountains, California-Oregon: U/Pb zircon and $^{40}Ar/^{39}Ar$ geochronology: Journal of Geophysical Research, v. 99, p. 4293–4321, doi:10.1029/93JB02061.

Hawkesworth, C.J., and Kemp, A.I.S., 2006, Using hafnium and oxygen isotopes in zircons to unravel the record of crustal evolution: Chemical Geology, v. 226, p. 144–162, doi:10.1016/j.chemgeo.2005.09.018.

Hillhouse, J.W., Gommé, C.S., and Vallier, T.L., 1982, Paleomagnetism and Mesozoic tectonics of the Seven Devils volcanic arc in northeastern Oregon: Journal of Geophysical Research, v. 87, p. 3777–3794.

Hirth, G., and Tullis, J., 1992, Dislocation creep regimes in quartz aggregates: Journal of Structural Geology, v. 14, p. 145–159, doi:10.1016/0191-8141(92)90053-Y.

Housen, B.A., and Dorsey, R.J., 2005, Paleomagnetism and tectonic significance of Albian and Cenomanian turbidites, Ochoco Basin, Mitchell Inlier, central Oregon: Journal of Geophysical Research, v. 110, p. B07102, doi:10.1029/2004JB003458.

Hrouda, F., and Kahan, Š., 1991, The magnetic fabric relationship between sedimentary and basement nappes in the High Tatra Mountains, N. Slovakia: Journal of Structural Geology, v. 13, p. 431–442, doi:10.1016/0191-8141(91)90016-C.

Iizuka, T., and Hirata, T., 2005, Improvements of precision and accuracy in in situ Hf isotope microanalysis of zircon using the laser ablation MC-ICPMS technique: Chemical Geology, v. 220, p. 121–137, doi:10.1016/j.chemgeo.2005.03.010.

Ishihara, S., 1977, The magnetite-series and ilmenite-series granitic rocks: Mining Geology, v. 27, p. 293–305, doi:10.11456/shigenchishitsu1951.27.293.

Ishihara, S., 2004, The redox state of granitoids relative to tectonic setting and Earth history: The magnetite-ilmenite series 30 years later: Transactions of the Royal Society of Edinburgh: Earth Sciences, v. 95, p. 23–33, doi:10.1017/S0263593300000894.

Johnson, K., and Schwartz, J.J., 2009, Overview of Jurassic–Cretaceous magmatism in the Blue Mountains Province (NE Oregon & W Idaho): Insights from new Pb/U (SHRIMP-RG) age determinations: Geological Society of America Abstracts with Programs, v. 41, no. 7, p. 182.

Johnson, K., Walton, C., Barnes, C.G., and Kistler, R.W., 1995, Time-dependent geochemical variations of Jurassic and Cretaceous plutons in the Blue Mountains, northeastern Oregon: Geological Society of America Abstracts with Programs, v. 27, no. 6, p. 435.

Johnson, K., Barnes, C.G., and Miller, C.A., 1997, Petrology, geochemistry, and genesis of high-Al tonalite and trondhjemites of the Cornucopia Stock, Blue Mountains, northeastern Oregon: Journal of Petrology, v. 38, p. 1585–1611, doi:10.1093/petroj/38.11.1585.

Johnson, K., Schwartz, J.J., and Walton, C., 2007, Petrology of the Late Jurassic Sunrise Butte pluton, eastern Oregon: A record of renewed Mesozoic arc activity?: Geological Society of America Abstracts with Programs, v. 39, no. 6, p. 209.

Kemp, A.I.S., Foster, G.L., Schersten, A., Whitehouse, M.J., Darling, J., and Storey, C., 2009, Concurrent Pb-Hf isotope analysis of zircon by laser ablation multi-collector ICPMS, with implications for the crustal evolution of Greenland and the Himalayas: Chemical Geology, v. 261, p. 244–263, doi:10.1016/j.chemgeo.2008.06.019.

Kurz, G.A., Schmitz, M.D., Northrup, C.J., and Vallier, T.L., 2012, U-Pb geochronology and geochemistry of intrusive rocks from the Cougar Creek complex, Wallowa arc terrane, Blue Mountains Province, Oregon-Idaho: Geological Society of America Bulletin, v. 124, p. 578–595, doi:10.1130/B30452.1.

Lalonde, A.E., and Bernard, P., 1993, Composition and color of biotite from granites: Two useful properties in the characterization of plutonic suites from the Hepburn internal zone of Wopmay orogen, Northwest Territories: Canadian Mineralogist, v. 31, p. 203–217.

LaMaskin, T.A., Dorsey, R.J., and Vervoort, J.D., 2008, Tectonic controls on mudrock geochemistry, Mesozoic rocks of eastern Oregon and western Idaho, U.S.A.: Implications for Cordilleran tectonics: Journal of Sedimentary Research, v. 78, p. 765–783, doi:10.2110/jsr.2008.087.

LaMaskin, T.A., Schwartz, J.J., Dorsey, R.J., Snoke, A.W., Johnson, K., and Vervoort, J.D., 2009, Mesozoic sedimentation, magmatism, and tectonics in the Blue Mountains Province, northeastern Oregon, *in* O'Connor, J.E., Dorsey, R.J., and Madin, I.P., eds., Volcanoes to Vineyards: Geological Field Trips through the Dynamic Landscape of the Pacific Northwest: Geological Society of America Field Guide 15, p. 187–202, doi:10.1130/2009.fld015(09).

Leake, B.E., 1978, Nomenclature of amphiboles: Canadian Mineralogist, v. 16, p. 501–520.

Lee, R.G., 2004, The geochemistry, stable isotopic composition, and U-Pb geochronology of tonalite trondhjemites within the accreted terrane, near Greer, north-central Idaho [MS thesis]: Washington State University, 132 p.

Ludwig, K.R., 2001, SQUID 1.02: A User's Manual: Berkeley Geochronology Center Special Publication 2, 21 p.

Ludwig, K.R., 2003, Isoplot 3: A Geochronological Toolkit for Microsoft Excel (rev. August 27, 2003): Berkeley Geochronology Center Special Publication 4, 70 p.

MacDonald, J.H., Jr., Harper, G.D., Miller, R.B., Miller, J.S., Mlinarevic, A.N., and Schultz, C.E., 2008, The Ingalls ophiolite complex, central Cascades, Washington: Geochemistry, tectonic setting, and regional correlations, *in* Wright, J.E., and Shervais, J.W., eds., Ophiolites, Arcs, and Batholiths: A Tribute to Cliff Hopson: Geological Society of America Special Paper 438, p. 133–159, doi:10.1130/2008.2438(04).

Malvoisin, B., Chopin, C., Brunet, F., and Galvez, M.E., 2012, Low-temperature wollastonite formed by carbonate reduction: A marker of serpentinite redox conditions: Journal of Petrology, v. 53, p. 159–176, doi:10.1093/petrology/egr060.

Manduca, C.A., Kuntz, M.A., and Silver, L.T., 1993, Emplacement and deformation history of the western margin of the Idaho batholith near McCall, Idaho: Influence of a major terrane boundary: Geological Society of America Bulletin, v. 105, p. 749–765, doi:10.1130/0016-7606(1993)105<0749:EADHOT>2.3.CO;2.

Matsell, L.J., Johnson, K., Schwartz, J.J., Richter, M.E., and Wooden, J.L., 2012, Garnet hornblendite blocks in serpentinite-matrix mélange in the Blue Mountains Province, NE Oregon: Geological Society of America Abstracts with Programs, v. 44, no. 6, p. 71.

McClelland, W.C., and Oldow, J.S., 2007, Late Cretaceous truncation of the western Idaho shear zone in the central North American Cordillera: Geology, v. 35, p. 723–726, doi:10.1130/G23623A.1.

Moyen, J.-F., Champion, D., and Smithies, R.H., 2010, The geochemistry of Archaean plagioclase-rich granites as a marker of source enrichment and depth of melting: Earth and Environmental Transactions of the Royal Society of Edinburgh, v. 100, p. 35–50, doi:10.1017/S1755691009016132.

Patchett, P.J., 1983, Importance of the Lu-Hf isotopic system in studies of planetary chronology and chemical evolution: Geochimica et Cosmochimica Acta, v. 47, p. 81–91, doi:10.1016/0016-7037(83)90092-3.

Patchett, P.J., and Tatsumoto, M., 1981, A routine high-precision method for Lu-Hf isotope geochemistry and chronology: Contributions to Mineralogy and Petrology, v. 75, p. 263–267, doi:10.1007/BF01166766.

Richter, M.E., and Johnson, K., 2014, The potential role of epidosite in water-saturated partial melting of mafic amphibolites: An example from Pollock Mountain, western Idaho: Geological Society of America Abstracts with Programs, v. 46, no. 5, p. 16.

Richter, M.E., Johnson, K., and Barnes, M.A.W., 2012, Migmatization of amphibolites on Pollock Mountain, Blue Mountains Province, western Idaho: Geological Society of America Abstracts with Programs, v. 44, no. 6, p. 71.

Scherer, E., Munker, C., and Mezger, K., 2001, Calibration of the lutetium-hafnium clock: Science, v. 293, p. 683–687, doi:10.1126/science.1061372.

Schwartz, J.J., and Johnson, K., 2009, Origin of paired Late Jurassic high and low Sr/Y magmatic belts in the Blue Mountains Province, NE Oregon: Geological Society of America Abstracts with Programs, v. 41, no. 7, p. 182.

Schwartz, J.J., Snoke, A.W., Frost, C.D., Barnes, C.G., Gromet, L.P., and Johnson, K., 2010, Analysis of the Wallowa-Baker terrane boundary: Implications for tectonic accretion in the Blue Mountains Province, northeastern Oregon: Geological Society of America Bulletin, v. 122, p. 517–536, doi:10.1130/B26493.1.

Schwartz, J.J., Snoke, A.W., Cordey, F., Johnson, K., Frost, C.D., Barnes, C.G., LaMaskin, T.A., and Wooden, J.L., 2011a, Late Jurassic magmatism, metamorphism, and deformation in the Blue Mountains Province, northeast Oregon: Geological Society of America Bulletin, v. 123, p. 2083–2111, doi:10.1130/B30327.1.

Schwartz, J.J., Johnson, K., Miranda, E.A., and Wooden, J.L., 2011b, The generation of high Sr/Y plutons following Late Jurassic arc-arc collision, Blue Mountains Province, NE Oregon: Lithos, v. 126, p. 22–41, doi:10.1016/j.lithos.2011.05.005.

Schwartz, J.J., Johnson, K., Mueller, P., Valley, J., Strickland, A., and Wooden, J.L., 2014, Time scales and processes of Cordilleran batholith construction and high-Sr/Y magmatic pulses: Evidence from the Bald Mountain batholith, northeastern Oregon: Geosphere, v. 10, p. 1456–1481, doi:10.1130/GES01033.1.

Snee, L.W., Lund, K., Sutter, J.F., Balcer, D.E., and Evans, K.V., 1995, An $^{40}Ar/^{39}Ar$ chronicle of the tectonic development of the Salmon River Suture Zone, western Idaho: U.S. Geological Survey Professional Paper 1438, p. 359–414.

Snee, L.W., Davidson, G.F., and Unruh, D.M., 2007, Geological, geochemical, and $^{40}Ar/^{39}Ar$ and U-Pb thermochronological constraints for the tectonic development of the Salmon River suture zone near Orofino, Idaho, *in* Kuntz, M.A., and Snee, L.W., eds., Geological Studies of the Salmon River Suture Zone and Adjoining Areas, West-Central Idaho and Eastern Oregon: U.S. Geological Survey Professional Paper 1738, p. 51–94.

Stacey, J.S., and Kramers, J.D., 1975, Approximation of terrestrial lead isotope evolution by a two stage model: Earth and Planetary Science Letters, v. 26, p. 207–221, doi:10.1016/0012-821X(75)90088-6.

Sun, S.S., and McDonough, W.F., 1989, Chemical and isotopic systematics of oceanic basalts: Implications for mantle composition and processes, *in* Saunders, A.D., and Norry, M.J., eds., Magmatism in the Ocean Basins: Geological Society of London Special Publication 42, p. 313–345, doi:10.1144/GSL.SP.1989.042.01.19.

Tarling, D.H., and Hrouda, F., 1993, The Magnetic Anisotropy of Rocks: London, Chapman and Hall, 217 p.

Tera, F., and Wasserburg, G.J., 1972, U-Th-Pb systematics in three *Apollo 14* basalts and the problem of initial Pb in lunar rocks: Earth and Planetary Science Letters, v. 14, p. 281–304, doi:10.1016/0012-821X(72)90128-8.

Tomkins, A.G., Rebryna, K.C., Weinberg, R.F., and Schaefer, B.F., 2012, Magmatic sulfide formation by reduction of oxidized arc basalt: Journal of Petrology, v. 53, p. 1537–1567, doi:10.1093/petrology/egs025.

Tulloch, A.J., and Kimbrough, D.L., 2003, Paired plutonic belts in convergent margins and the development of high Sr/Y magmatism: Peninsular Ranges Batholith of Baja California and Median Batholith of New Zealand, *in* Johnson, S.E., Paterson, S.R., Fletcher, J.M., Girty, G.H., Kimbrough, D.L., and Martín-Barajas, A., eds., Tectonic Evolution of Northwestern México and the southwestern USA: Geological Society of America Special Paper 374, p. 275–295, doi:10.1130/0-8137-2374-4.275.

Unruh, D.M., Lund, K., Snee, L.W., and Kuntz, M.A., 2008, Uranium-lead zircon ages and Sr, Nd, and Pb isotope geochemistry of selected plutonic rocks from western Idaho: U.S. Geological Survey Open File Report 2008-1142, 42 p.

Vallier, T.L., 1995, Petrology of pre-Tertiary igneous rocks in the Blue Mountains region of Oregon, Idaho, and Washington: Implications for the geologic evolution of a complex island arc, *in* Vallier, T.L., and Brooks, H.C., eds., Geology of the Blue Mountains Region of Oregon, Idaho, and Washington: Petrology and Tectonic Evolution of Pre-Tertiary Rocks of the Blue Mountains Region: U.S. Geological Survey Professional Paper 1438, p. 125–209.

Vervoort, J.D., Patchett, P.J., Söderlund, U., and Baker, M., 2004, The isotopic composition of Yb and the precise and accurate determination of Lu concentrations and Lu/Hf ratios by isotope dilution using MC-ICPMS: Geochemistry, Geophysics, Geosystems, v. 5, p. Q11002, doi:10.1029/2004GC000721.

Walker, N.W., 1989, Early Cretaceous initiation of post-tectonic plutonism and the age of the Connor Creek fault, northeastern Oregon: Geological Survey of America Abstracts with Programs, v. 21, p. 155.

Weinberg, R.F., and Hasalová, P., 2015, Water-fluxed melting of the continental crust: A review: Lithos, v. 212–215, p. 158–188, doi:10.1016/j.lithos.2014.08.021.

Williams, I.S., 1998, U-Th-Pb geochronology by ion microprobe, *in* McKibben, M.A., Shanks W.C., III, and Ridley, W.I., eds., Applications of Microanalytical Techniques to Understanding Mineralizing Processes: Reviews in Economic Geology Special Publication 7, p. 1–35, doi:10.5382/Rev.07.01.

Wilson, D., and Cox, A., 1980, Paleomagnetic evidence for tectonic rotation of Jurassic plutons in Blue Mountains, eastern Oregon: Journal of Geophysical Research, v. 85, p. 3681–3689, doi:10.1029/JB085iB07p03681.

Winther, K.T., and Newton, R.C., 1991, Experimental melting of hydrous low-K tholeiite: Evidence on the origin of Archaean cratons: Bulletin of the Geological Society of Denmark, v. 39, p. 213–228.

Wolf, M.B., and Wyllie, P.J., 1993, Garnet growth during amphibolite anatexis: Implications of a garnetiferous restite: The Journal of Geology, v. 101, p. 357–373, doi:10.1086/648229.

Woodhead, J.D., Hergt, J., Shelley, M., Eggins, S., and Kemp, R., 2004, Zircon Hf-isotope analysis with an excimer laser, depth profiling, ablation of complex geometries, and concomitant age estimation: Chemical Geology, v. 209, p. 121–135, doi:10.1016/j.chemgeo.2004.04.026.

Wu, F.Y., Yang, Y.H., Xie, L.W., Yang, J.H., and Xu, P., 2006, Hf isotopic compositions of the standard zircons and baddeleyites used in U-Pb geochronology: Chemical Geology, v. 234, p. 105–126, doi:10.1016/j.chemgeo.2006.05.003.

Žák, J., Verner, K., Johnson, K., and Schwartz, J.J., 2012, Magnetic fabric of Late Jurassic arc plutons and kinematics of terrane accretion in the Blue Mountains, northeastern Oregon: Gondwana Research, v. 22, p. 341–352, doi:10.1016/j.gr.2011.09.013.

Manuscript Accepted by the Society 1 July 2015
Manuscript Published Online 6 November 2015

Geological Society of America Special Papers

Composite Sunrise Butte pluton: Insights into Jurassic–Cretaceous collisional tectonics and magmatism in the Blue Mountains Province, northeastern Oregon

Kenneth Johnson, Joshua J. Schwartz, Jirí Zák, et al.

Geological Society of America Special Papers 2015;513; 377-398 , originally published onlineNovember 6, 2015
doi:10.1130/2015.2513(10)

Notes